# International Journal of Engineering (IJE)

ISSN : 1985-2312

VOLUME 4, ISSUE 6

PUBLICATION FREQUENCY: 6 ISSUES PER YEAR

# International Journal of Engineering (IJE)


## Volume 4, Issue 6, 2011

**Edited By**
**Computer Science Journals**
**www.cscjournals.org**

**Editor in Chief Dr. Kouroush Jenab**

# International Journal of Engineering (IJE)

Book: 2011 Volume 4, Issue 6

Publishing Date: 08-02-2011

Proceedings

ISSN (Online): 1985-2312



IJE Journal is a part of CSC Publishers

http://www.cscjournals.org



Published in Malaysia

Typesetting: Camera-ready by author, data conversation by CSC Publishing Services – CSC Journals, Malaysia

**CSC Publishers**

# Editorial Preface

This is the fifth issue of volume four of International Journal of Engineering (IJE). The Journal is published bi-monthly, with papers being peer reviewed to high international standards. The International Journal of Engineering is not limited to a specific aspect of engineering but it is devoted to the publication of high quality papers on all division of engineering in general. IJE intends to disseminate knowledge in the various disciplines of the engineering field from theoretical, practical and analytical research to physical implications and theoretical or quantitative discussion intended for academic and industrial progress. In order to position IJE as one of the good journal on engineering sciences, a group of highly valuable scholars are serving on the editorial board. The International Editorial Board ensures that significant developments in engineering from around the world are reflected in the Journal. Some important topics covers by journal are nuclear engineering, mechanical engineering, computer engineering, electrical engineering, civil & structural engineering etc.

The coverage of the journal includes all new theoretical and experimental findings in the fields of engineering which enhance the knowledge of scientist, industrials, researchers and all those persons who are coupled with engineering field. IJE objective is to publish articles that are not only technically proficient but also contains information and ideas of fresh interest for International readership. IJE aims to handle submissions courteously and promptly. IJE objectives are to promote and extend the use of all methods in the principal disciplines of Engineering.

IJE editors understand that how much it is important for authors and researchers to have their work published with a minimum delay after submission of their papers. They also strongly believe that the direct communication between the editors and authors are important for the welfare, quality and wellbeing of the Journal and its readers. Therefore, all activities from paper submission to paper publication are controlled through electronic systems that include electronic submission, editorial panel and review system that ensures rapid decision with least delays in the publication processes.

To build its international reputation, we are disseminating the publication information through Google Books, Google Scholar, Directory of Open Access Journals (DOAJ), Open J Gate, ScientificCommons, Docstoc and many more. Our International Editors are working on establishing ISI listing and a good impact factor for IJE. We would like to remind you that the success of our journal depends directly on the number of quality articles submitted for review. Accordingly, we would like to request your participation by submitting quality manuscripts for review and encouraging your colleagues to submit quality manuscripts for review. One of the great benefits we can provide to our prospective authors is the mentoring nature of our review

process. IJE provides authors with high quality, helpful reviews that are shaped to assist authors in improving their manuscripts.

**Editorial Board Members**
International Journal of Engineering (IJE)

# Editorial Board

# Table of Content

Volume 4, Issue 6, December 2011

## Pages

# Modeling of Gas Turbine Co-Propulsion Engine to Ecotourism Vessel for Improvement of the Sailing Speed

**O. Sulaima** o.sulaiman@umt.edu.my
*Department of Maritime Technology,*
*Faculty of Maritime Studies and Marine Science,*
*University Malaysia Terengganu, Terengganu, Malaysia*

**H. Saharuddin**
*Department of Maritime Technology,*
*Faculty of Maritime Studies and Marine Science,*
*University Malaysia Terengganu, Terengganu, Malaysia*

**A.S.A.kader** abdsaman@fkm.edu.my
*Department of Mechanical Engineering,*
*University Technology Malaysia,*
*Skudai, Johor. Malaysia*

**M.Zamani**
*Department of Mechanical Engineering,*
*University Technology Malaysia,*
*Skudai, Johor. Malaysia*

**Abstract**

Sailing speed is important an factor in choosing marine engines. The uses of gas turbine as co-propulsion engine for improving sailing speed of ecotourism vessels to fulfill requirement of SAR operation. Gas turbine co-propulsion engine have an advantage of high power to weight ratio in comparative to other heat engines. This paper presents the results and study on diesel engine, simple cycle gas turbine and regenerative gas turbine performances The relation between the thermal efficiency of heat engine to fuel consumption is used to estimate fuel consumption rate. The design of heat engine can be determined the specific heat ratio and pressure ratio of the operation cycle which will give necessary impacts to the thermal efficiency of the heat engine. Results from the numerical calculation for the implementation of gas turbine will provide he decision support. The paper also discusses the impact of co-propulsion engine to the ships stability and proper power rating of gas turbine co-propulsion engine estimated by numerical calculation in order to achieve maximum sailing speed up to 35 knots.

**Keywords:** Gas Turbine, Regeneration, Sailing Speed Thermal Efficiency, Fuel Consumption

## 1. INTRODUCTION

The sailing speed of ecotourism can be improved by several methods. In this research implementation of gas is proposed as co-propulsion engine to improve the ecotourism vessel sailing speed up to 35knots. The vessel under study is the important transport connecting the mainland from Mersing jetty to Tioman Island. High speed sailing is necessary for the vessel to

carry out the search and rescueoperation in open sea under emergency circumstances. Besides, improving passenger ferry sailing speed will overcome the problem of vessels shiftment delays during peak season inMay.

Gas turbine also called a combustion turbine is a rotary engine that extracts energy from a flow of combustion gas. In order to adapt the function, the gas turbine composes of four important components, which are compressor, combustion chamber, turbines and exhaust. Energy is added to gas stream by combustor through ignition of the mixture of atomized fuel and air. The gaseous streams are then directed through a nozzle toward a turbine. The hot gases stream will spin the turbine and empower the compressor.

Comparative to others heat engine, gas turbine will have the advantages of high power to weight ratio. The gas turbine provides the same output power as the diesel engine having more compact design and smaller in sizes and weight in comparison with diesel engine. However, under certain circumstances, the diesel engine will show higher in fuel efficiency in comparative to gas turbine [1, 2].

The design of gas turbine will give impacts to the performances of gas turbine. Design must take into account on specific heat ratio and the pressure ratio in order to produce high performance gas turbine co-propulsion engine. These two variables give significant change of thermal efficiency of gas turbine co-propulsion engine.

## 2. MODELLING PROCESS

The thermodynamic properties of the each heat engine were emphasized three types of heat engine were selected and put into study. Diesel cycle, Bryton cycle and combine cycle are studies to examine the properties of individual heat engine.

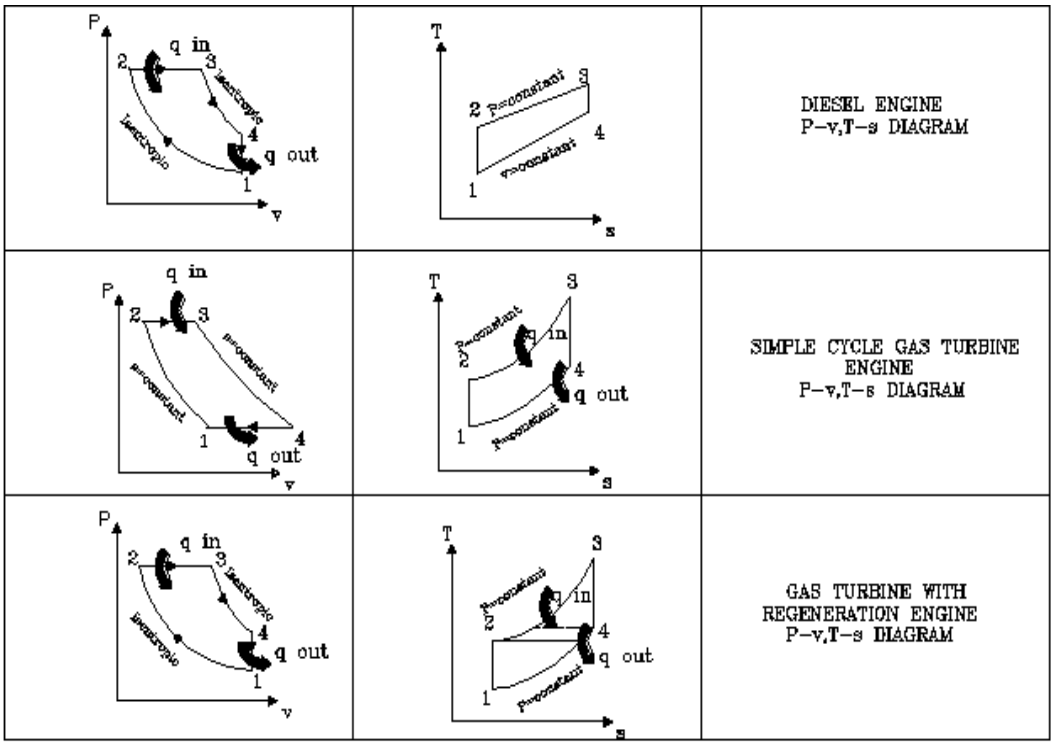


**FIGURE 1:** thermodynamic properties of co-propulsion engine

A survey is done by a visiting the passenger Fast Ferry Company located at Mersing jetty, Johor. Data collections are done on the vessel understudy. These included ship's particular general arrangement, propulsion engine specification, sailing speeds and fuel consumption rate [3,4].

The thermodynamic properties of the following heat engine were presented in curve to examine the properties of each heat engine. The plotting tools; Mathlab is applied for plotting purposes. The thermodynamic formula needs to translate to the M-code in order to present a relation curve [5,6]. Table 1-4 show the M-code for propulsion engines.

**TABLE1:** Thermal efficiency of co-propulsion engine

| Types of co-propulsion engine | Thermal efficiency formula |
|---|---|
| Diesel engine | $n_{th,diesel} = 1 - \frac{1}{r^{k-1}}[\frac{r_c{}^k - 1}{k(r_c - 1)}]$ |
| Simple cycle Gas turbine | $n_{th\ bryton} = 1 - \frac{1}{r_p{}^{(k-1)/k}}$ |
| Regeneration gas turbine | $n_{th\ regen} = 1 - \left(\frac{T_1}{T_3}\right)(r_p)^{k(k-1)}$ |

**TABLE 2:** M-code for Diesel engine

```
%M
code for thermodynamic properties of diesel engine
k=1.4;                                          r=[2:2:24];
rco=2;                                          a=r.^(k
1);                                             b=(rco^k)
1;                                              c=k*(rco
1);                                             e=b./(a*c);
nD=1
e;                                              plot(r,nD,'red');
legend('at k=1.4');                             xlabel('compress
ratio,r');                                      ylabel('Dieselefficiency,nD');
title('thermal efficiency vs comprssion ratio');
```

**TABLE 3:** M-code for simple cycle gas turbine

```
%M-code for thermodynamic properties of simple gas turbine
k=1.4;                                          rp=[1:2:24];
x=(k-1)/k;                                      nB=1-
rp.^-xplot(rp,nB,'magenta');                    xlabel('pressure ratio,rp');
ylabel('Thermal efficiency,nB');                legend('at
k=1.4');                                        title('Thermal
efficiency of gas turbine vs pressure ratio');
```

**TABLE 4:** M-code for regeneration gas turbin

```
%M-code for thermodynamic properties of regeneration gas turbine
k=1.4;
r=[1:2:50];
t=0.5;
x=(k-1)/k;
nR=1-t*(r.^x);
plot(r,nR,'black');
xlabel('pressure ratio,r');
ylabel('Thermal efficiency,n');
legend('regen turbine at k=1.4');

title('regen gas turbine thermal efficiency');
```

The fuel consumption rate of each heat engine will then translate from the thermal efficiency using formula state below:

$$Fuel\ consumption = \frac{\left(\frac{EHP}{\eta_{th}}\right)}{net\ heating\ value\ of\ diesel}$$

After determining the types of co-propulsion engine to implement, the power output selection can be performed by numerical calculation by using the related formula follow the sequence as shown in Figure 2.

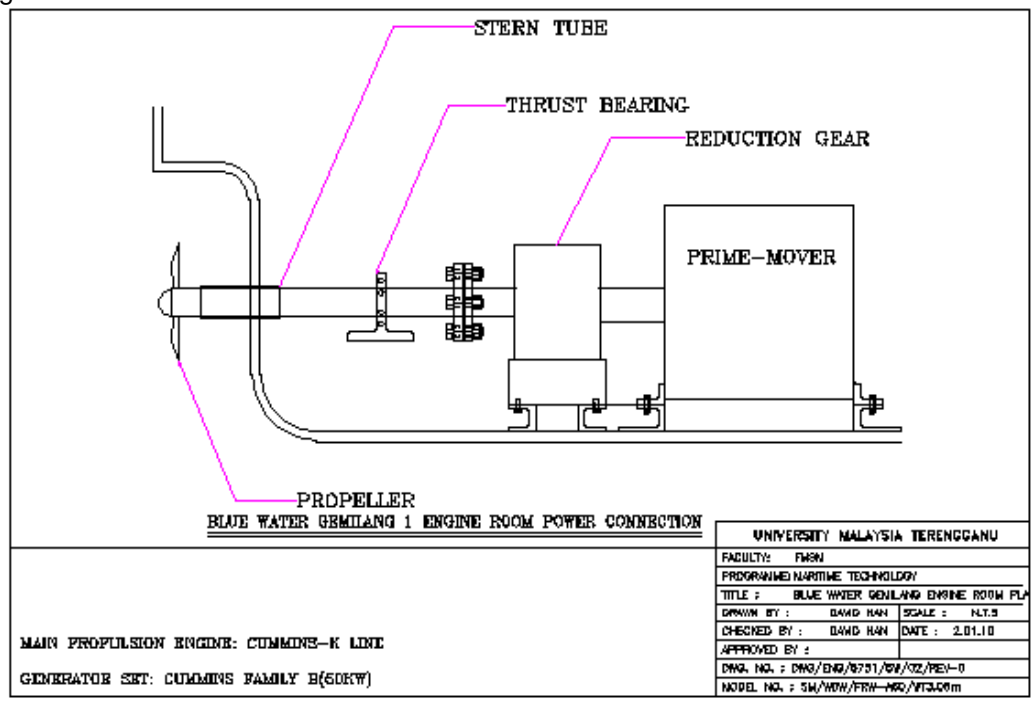


**FIGURE 2:** Arrangement of machinery onboard ship

**TABLE5:** Formula for numerical power calculation

| Types of power | Simplified | Formula |
|---|---|---|
| Effective horse power (EHP) | EHP=RV | Effective horse power required to tow a hull without a propeller. |
| Thrust horsepower (THP) | $THP = T \times V_a$ | thrust horsepower is power delivered by propeller to the water |
| Delivered Horsepower | $DHP = \frac{THP}{\eta_p}$ | Delivered horsepower (DHP) is the power that is delivered by the shaft to the propeller. |

| | | |
|---|---|---|
| Shaft horsepower | $SHP = \frac{DHP}{n_B\, n_S} = \frac{DHP}{n_M}$ | Shaft horse power is the power delivered by engine to the shaft after gearing and thrust bearing. |
| Brake horse power | $BHP = \frac{SHP}{n_G}$ | The power delivered by the prime mover at its connection flange is called brake horsepower. |

## 3. RESULT AND DISCUSSION

The data acquired during the survey are presented in tablelar form. The table 6 below shows the detail of the passenger ferry company. Bluewater Express ferry services are a company established in 1999. The core business offered are the ferry services to the passengers coming to Pulau Tioman. The company currently owned 8 fast ferries for the passenger services. Besides, the company owned a few cargo ships modified from the ordinary fisherman boat to transfer cargoes in between Pulau Tioman to the mainland to full fill the demands in the Tioman Island. (Refer to Table 6, and Table 7).

**TABLE 6:** Details of the ferry company

| | | |
|---|---|---|
| 1 | Company name: | BlueWater Express |
| 2 | Location: | Mersing,Johor |
| 3 | Name of Company's owner: | En.Rizam Bin Ali |
| 4 | Types of business: | passenger fast ferry |
| 5 | Routine: | Mersing jetty to Tioman |
| 6 | Distance: | 35n miles |
| 7 | Name of Vessel: | Gemilang 1 |
| 8 | Types of vessel: | Fiber single hull vessel |
| 9 | Vessel Manfacturer: | PT.Bintan Shipping Bioteknik Tanjung Pinang Shipyard |
| 10 | Maximum number passenger: | 100 passengers |

**TABLE 7:** Ship Hull details

| | | |
|---|---|---|
| 1 | Length overall | 23.7m |
| 2 | beam | 5.20m |
| 3 | draft | 2.20m |
| 4 | Hull types: | Single hull |
| 5 | Materials | Fiber class |
| 6 | Detail of lighting system | 12fluerecent light(45watt),12 others light bulb(24watt) |
| 7 | Number of pump required | 6 batt pump,1 electrical pump,2 mechanical pump(ramp pump) |
| 8 | Vessel average sailing speed | 20knots |
| 9 | DWT(base on dimension) | 271.2tonnes |

The vessel under studies named Gemilang 1. The vessel was constructed by PT. Bintan Shipping Bioteknik in Tanjung Pinang, Indonesia. The ship hull has the dimension as shown in the Table. The machinery used onboard was drafted for the reason of recommendation on the implementation of co-propulsion engine ( See Figure 3 and 4 ).

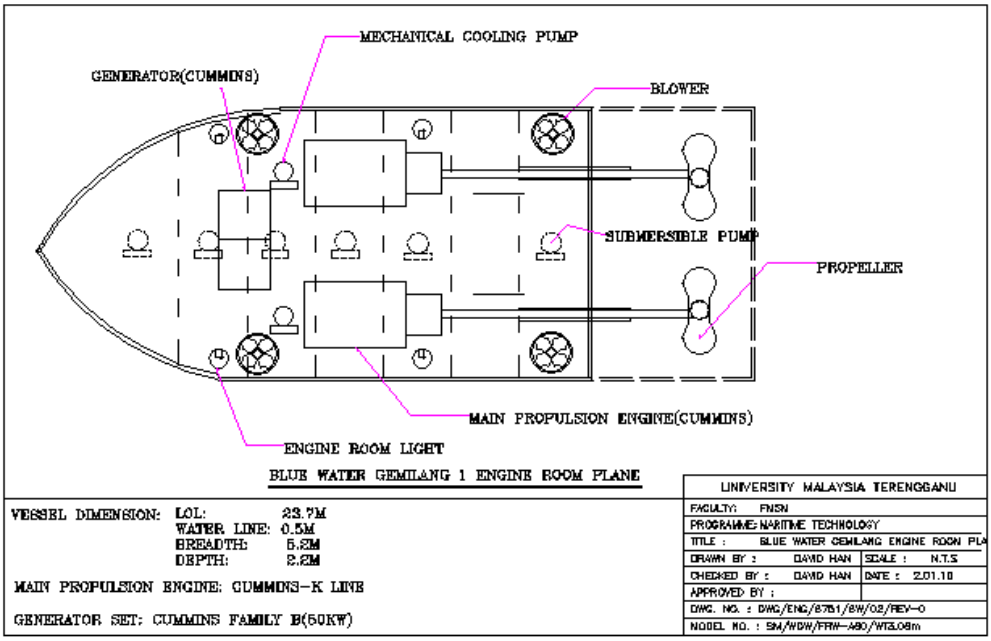


**FIGURE 3:** Machinery arrangement in Gemilang 1 engine room

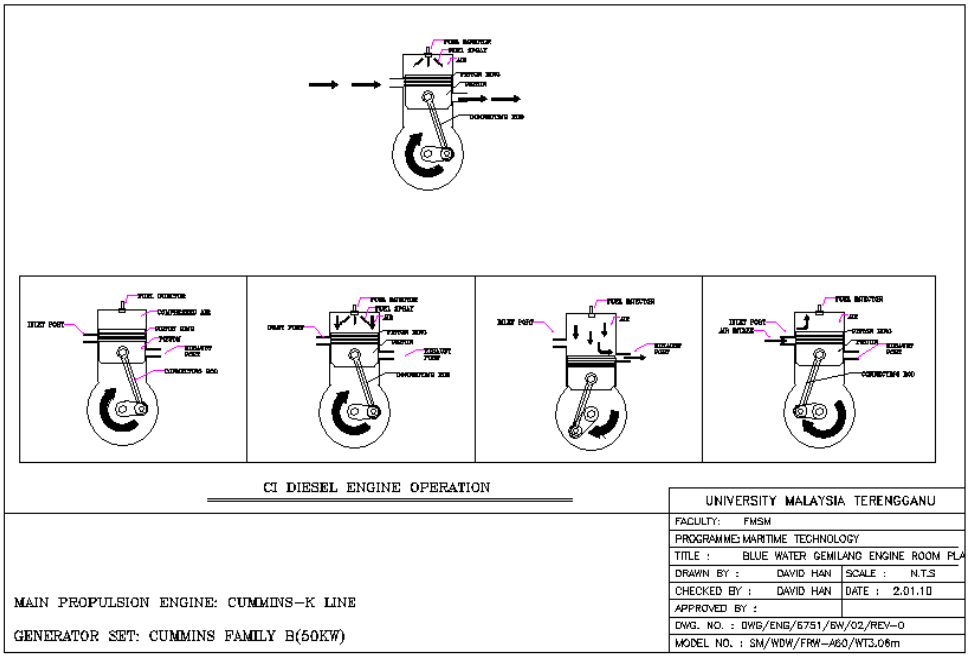


**FIGURE 4:** Mechanism of CI diesel propulsion engine in Gemilang 1

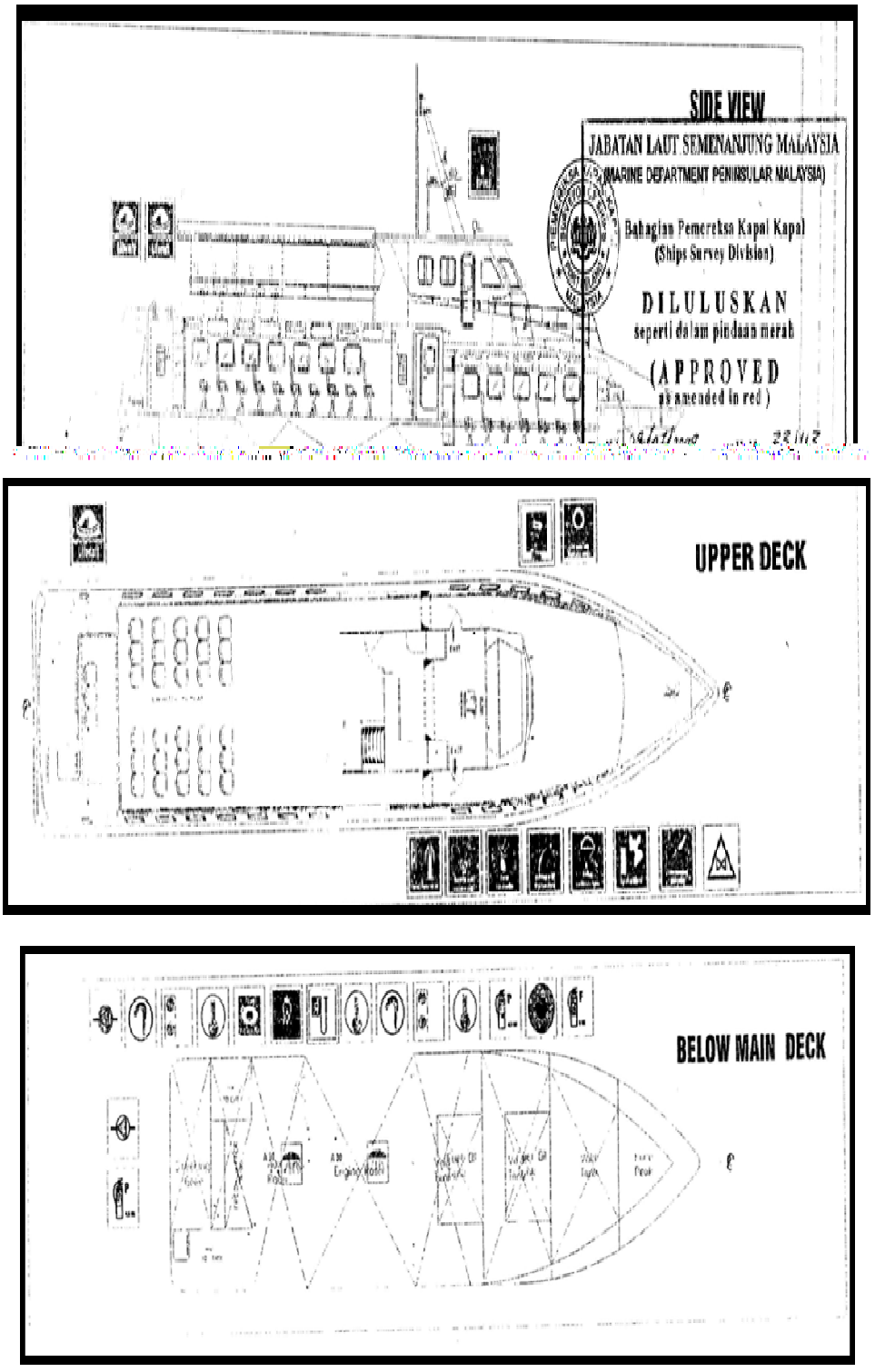


**FIGURE 5:** GA-plan of Gemilang 1 (general arrangement plan)

Gemilang1 is equipped with 2 propulsion engines and capable to propel the ship at sailing speed up to 20 knots. In order to fulfill the demand of the machinery that is necessary for sailing the desired sailing speed, redundant systems such as water pump system, lighting system, and the

electronics devices for the navigational purposes are installed. The vessel is also equipped with a generator power rating up to 50kW. The properties of the propulsion engine are presented in the Table 8 below.

**TABLE 8:** Propulsion engine specification

| | ENGINE DETAILS: | DESCRIPTION: |
|---|---|---|
| 1 | Engine model: | KTA-M4 Marine propulsion engine |
| 2 | Engine types: | IN-LINE, 6 CYLINDER, 4 STROKE DIESEL |
| 3 | Bore & stroke: | 159 mm x 159 mm (6.25 in x 6.25 in) |
| 4 | Displacement: | 19 L (1150 in3) |
| 5 | Rotational direction: | COUNTERCLOCKWISE FACING FLYWHEEL |
| 6 | Aspiration: | TURBOCHARGED/AFTERCOOLED |
| 7 | Fuel consumption: | 135.1 (35.7)Rated. 94.6 (25.0)ISO |
| 8 | Number of engine used: | 2pcs |
| 9 | Rating definition: | HEAVY DUTY |
| 10 | Emission : | IMO STANDARD |
| 11 | Engine rotation(RPM) : | 2100revolution per second |
| 12 | Power rating: | 522kW |

In predicting the efficiency of gas turbine and diesel engine, assumption has been made in order to standardize the condition at where the cycles performed. In comparing the performance of gas turbine versus diesel engine; we need to make some assumption on the working fluid for both of the system. The air is necessary in carrying out the combustion process. Fresh air entering the combustion chamber was considered under the cold air standard assumptions[10, 11]. Where by the specific heat ratio k, is represented by k=1.4 (specific heat ratio value under room temperature) (See Figure 6).

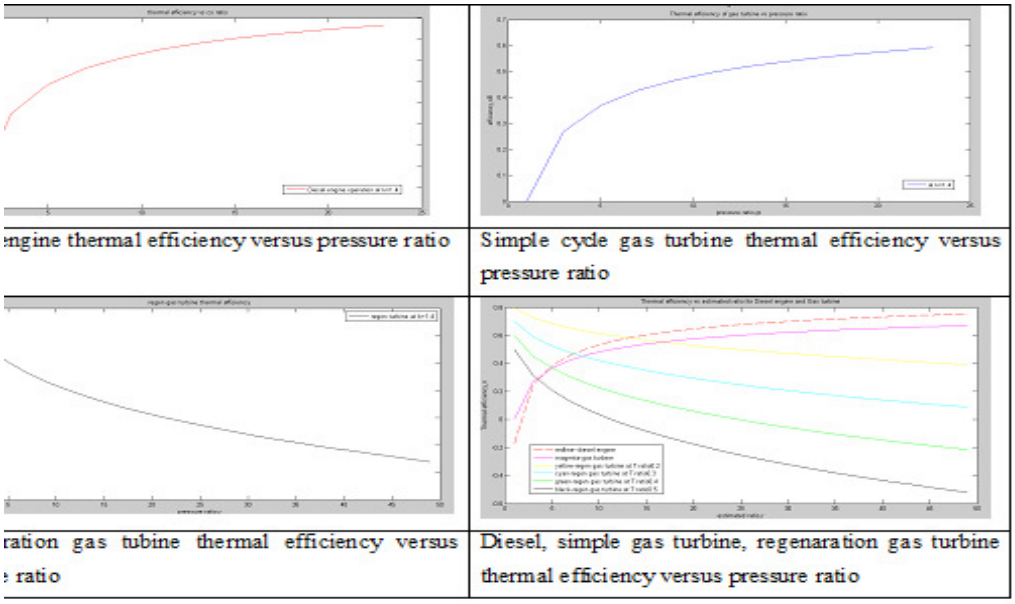


**FIGURE 6:** Thermal efficiency of each types co-propulsion engine

Besides, assumption is made on that the pressure ratio and cutoff ratio are similar in term of working condition. Compression ratio r, is defined as the ratio of the volume of its combustion chamber; from its largest capacity to its smallest capacity. It is a fundamental specification for many common combustion engines. While the pressure ratio $r_p$, for gas turbine is defined as ratio of the pressure at the core engine exhaust and fan discharge pressure compared to the intake pressure to the gas turbine engine.

$$r_p = \frac{p_2}{p_1} = \frac{v_1}{v_2} = r$$

$$r_p = r_c = r_A$$

Where:

$r_A = Estimated\ ratio\ on\ working\ condition$

The study involved the feasibility of implementing a gas turbine to improve the vessel sailing speed up to 35 knots. The study relates the operation of the gas turbine and diesel engine with thermal efficiency of the cycle.

Figure 7 illustrates the relation between thermal efficiency with pressure ratio for simple cycle of gas turbine and diesel engine. It shows that at the early state of the curve, gas turbine show steeper increment in thermal efficiency with the increasing pressure ratio.

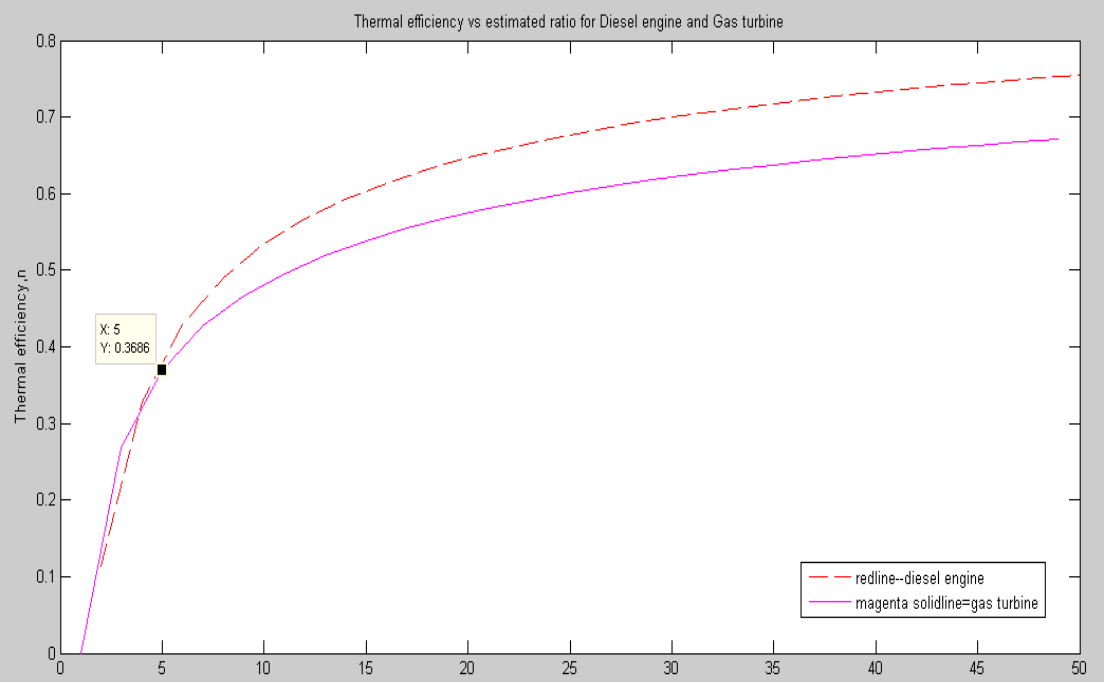


**FIGURE 7:** Thermal efficiency of each types co-propulsion engine

The performance of gas turbine and diesel engine overlaps at pressure ratio 5. In the middle state of the curve, the diesel engine has higher thermal efficiency with the increasing pressure ratio. From the curve shown, it is observed that the simple cycle gas turbine engine is less efficient in comparison to diesel engine.

The gas turbine operation can be improved by applying the regeneration cycle. The temperature of exhaust gas leaving the turbine is higher than the temperature of the air leaving the compressor. By leading the heat exhaust gaseous through the heat recuperates to preheat the compressed air from the compressor can improve the thermal efficiency of the gas turbine. Figure 8 shows the thermal efficiency curve between diesel engine, simple cycle gas turbine and the regenerative gas turbine at variable temperature ratio [6, 7].

Figure 8 illustrates the regenerative gas turbine with the minimum temperature ratio between the exhaust gas and the compressed air shows higher thermal efficiency in the early stage, the thermal efficiency of the following gas turbine decrease gradually with the increasing of the pressure ratio. From the diagram it is that the gas turbine withregenraton is the ideal selection for the co-propulsion engine because it shows high thermal efficiency in low pressure ratio. Low

pressure ratio carries significant information of low back work ratio and horse power of the following engine [8, 9].

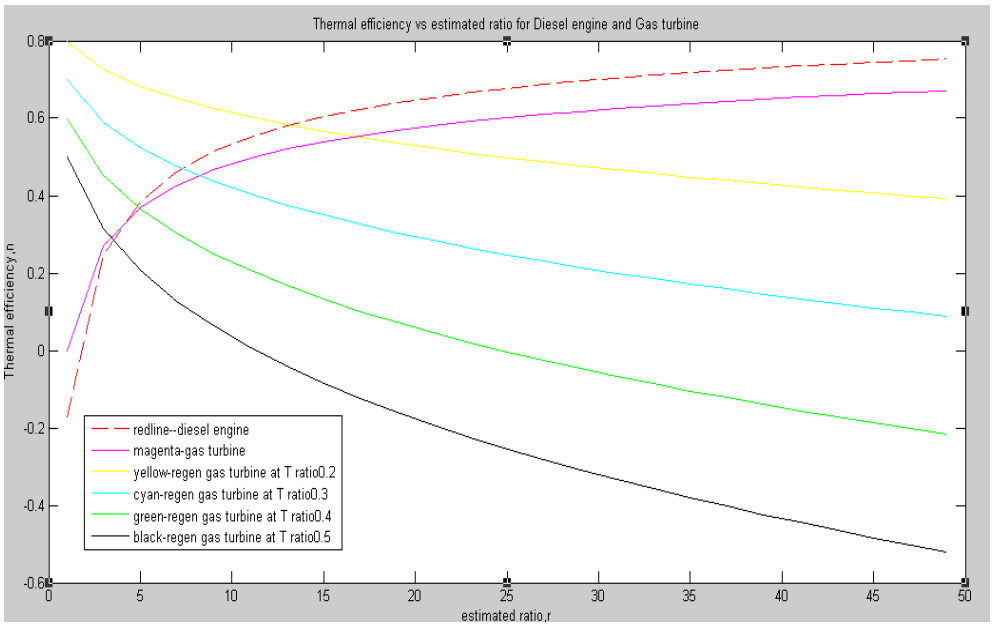


**FIGURE 8:** Thermal efficiency of each types co-propulsion engine

## Fuel consumption of co-propulsion engine

The fuel consumption always the criteria to consider during the marine engine selection, the optimum usage of fuel will ensure profits to the passenger company. By using the formula as stated below, the thermal efficiency of co-propulsion engine can be interrelated.

$$Fuel\ consumption = \frac{\left(\frac{3415Btu}{\eta_{th}}\right)}{net heating\ value\ of\ diesel}$$

In this case, we select the diesel fuel as the source for the heat engine. The diesel fuel having the net heating value of 130000btu/gallon. Substitute the net heating value, then the fuel consumption rate can be represented by the curve plotted by MATLAB as shown in Figure 9.

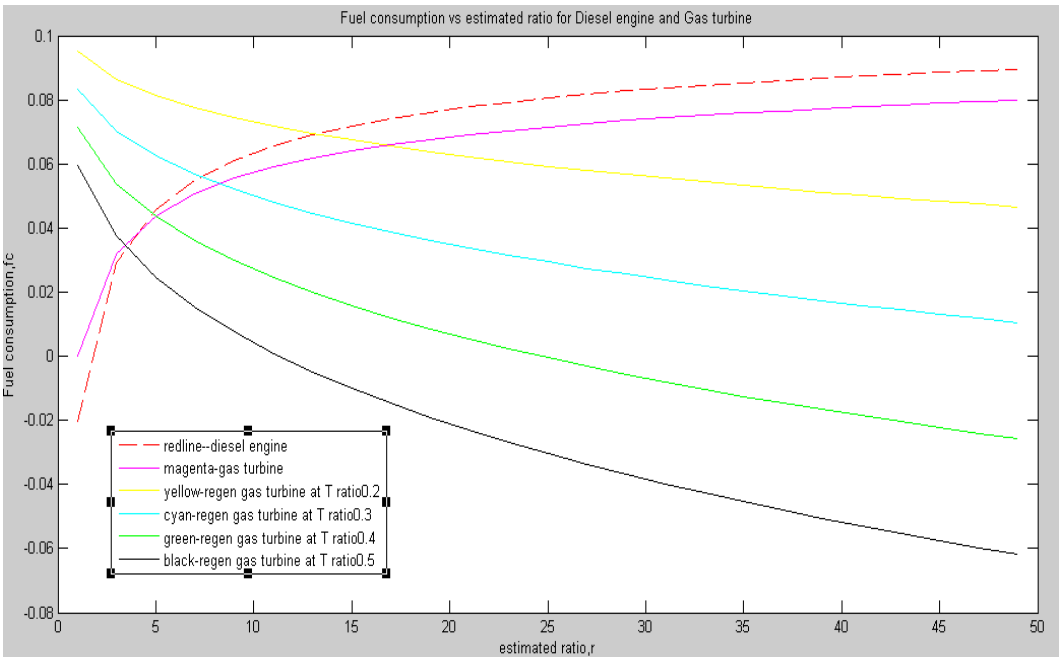


**FIGURE 9:** Fuel consumption (gallon) of each types co-propulsion engine

From the curve shown in Figure 9 it can be concluded that the fuel consumption rate versus estimated ratio for the diesel engine, simple cycle gas turbine, and regenerative gas turbine shows the similar trend. The regeneration gas turbine with the temperature ratio 0.3 showing a moderate fuel spent over the power production. Hence, the regenerative gas turbine will be the ideal selection as co-propulsion engine among the others. Location for the regeneration gas turbine in engine room [8, 10].

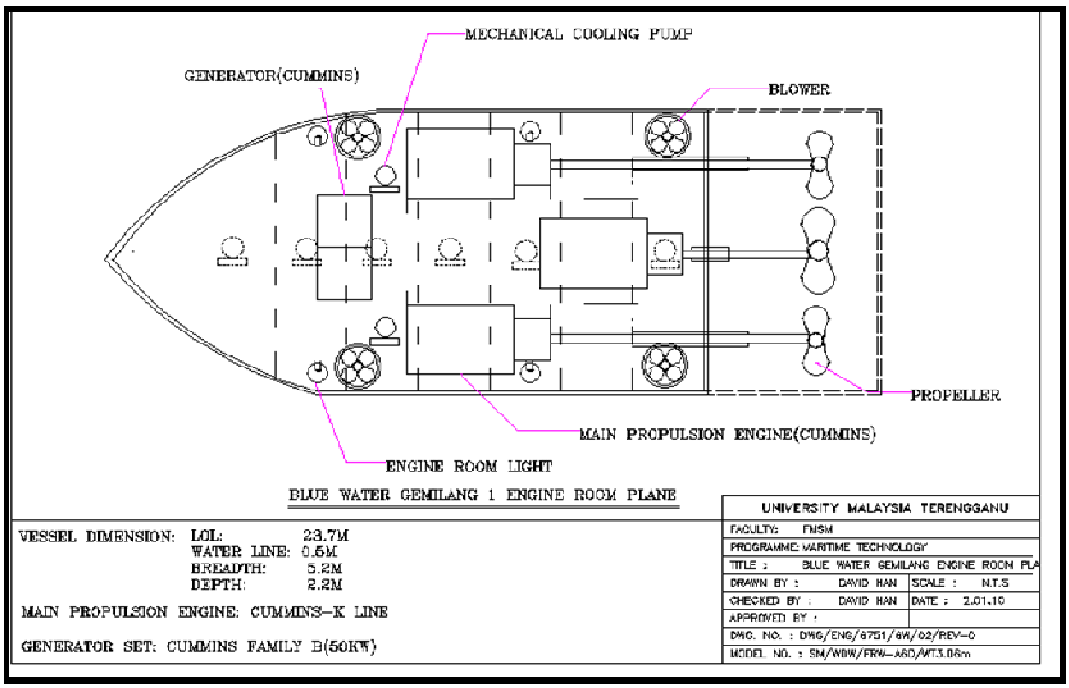


**FIGURE 10:** Recommendation for distribute the co-propulsion engine

### 3.2 Power calculation

The current existing diesel engines remain as a main propulsion engine to sail the ship at economic speed. The minimum power required to propel the vessel is computed theoretically. The numerical modeling involve assumption on the numbers of crews, weight of luggage and cargoes carried to estimate the dead weight tones of the vessel under studies. The brake horse power obtained base on theoretical calculation at variable speed is shown in the Table 9.

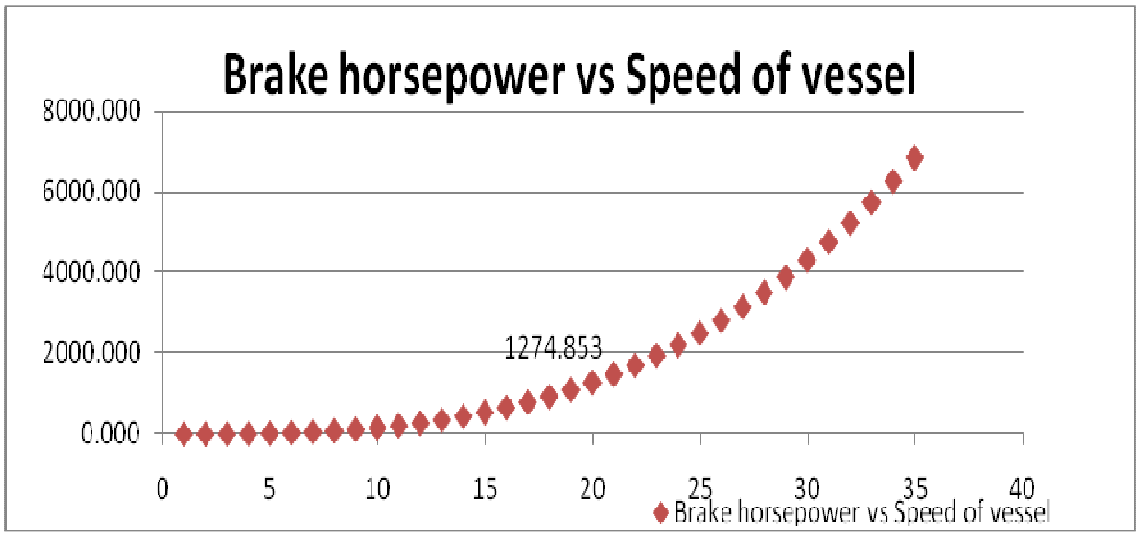


**FIGURE 11:** Brake horse power at various speeds

**TABLE 9:** Validation on the power calculation

| Description | Theoretical calculation | Engine applied onboard ship |
|---|---|---|
| Value (HP) | 1274.85hp | 1400hp |
| Value (kW) | 950.66kW | 1043.98kW |

From the diagram the power rating of the diesel engine calculated based on theoretical calculation are closed to the diesel engines currently applied on that following vessel. From the survey, we knew that there were 2 diesel engines with power rating of 700hp each applied on the vessel to propel the vessel to sail at optimum speed. On economy aspect, the selection of higher horsepower propulsion engines is necessary for the vessel to sail at optimum speed instead of sailing a vessel with full speed at engine maximum performances. The speed control can be done by adjusting on the throttling valve located at fuel pump attached to diesel engine. Besides, in real environment, there are some other factors to take into consideration. Air resistant due to the size of the superstructure of the vessel may require higher power propulsion to propelling the vessel to move forward [11,12].

For the co-propulsion engine, the output power becomes the terminology chosen in select the marine engine. Referring to the curve shown, the resistances of the vessel differ at variable speed. Hence, numerical calculation on the power at various speeds is necessary in order to ensure the vessel can sail at desired speed (See Figure 12).

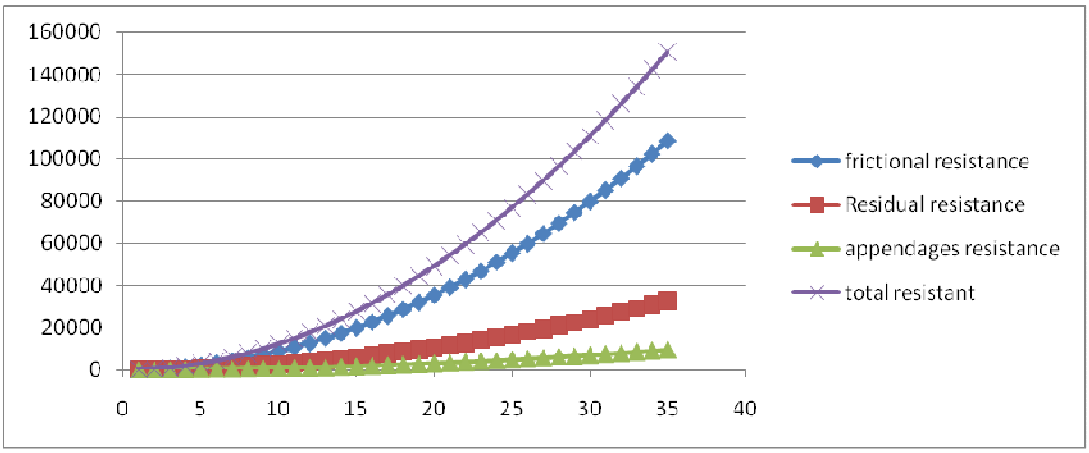


**FIGURE 12:** Types of resistances at variable speed

Figure13 shows the types of power at various speed. The minimum power required to propel a vessel to move forward is the effective horse power. The brake horsepower is the highest power and will encounter power loss in each transition state from the engine to the shaft following with the propeller.

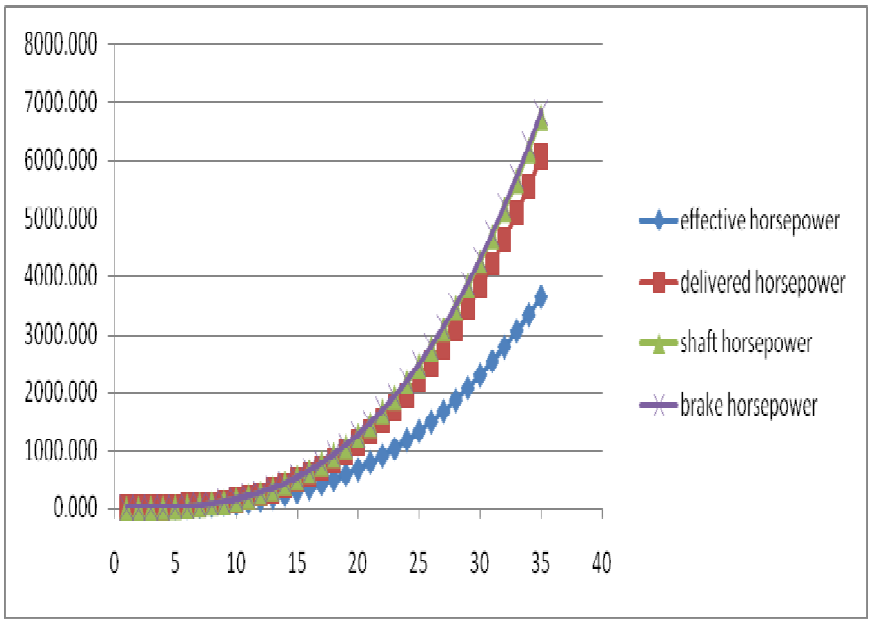


**FIGURE 13:** Types of power at variable speed

The result from the numerical calculation on the power output of co-propulsion engine shown that the minimum brake horsepower required for the co-propulsion engine is 1274.85hp.The recommended horse power for co-propulsion to implement is 1300hp.That is 10% margin of power excess to suit the speed of vessel. The regeneration gas turbine is selected after performing the analysis by plotting curve. The exhaust gas released by regeneration gas turbine was retracted and used to reheat the compressed gas existing from the compressor.

The paper aimed to improve ecotourism vessel sailing speed by implement a gas turbine as co-propulsion engine. The objective of the to improve the speed of vessel up to 35 knots with minimum fuel consumption is demonstrated in the power curve. Numerical calculation on the power output of co-propulsion engine shown that the minimum brake horsepower required for the co-propulsion engine is 6263.35hp 13,14]. The recommended horse power for co-propulsion to

implement is ranging from 6890hp up to 6900 hp. That is 10% margin of power excess to suit the speed of vessel. The result of regenerative gas turbine have an advantages by reduces the heat release to the environment. In economy aspect, although gas turbine co-propulsion engine display higher initial cost, but the lower operating and maintenances cost will reduced the payback period of the following investment.

**4.0 CONCLUSION**

The paper proposed to improve ecotourism vessel sailing speed by implementing a gas turbine as co-propulsion engine. The study of feasibility of implementing a gas turbine as co-propulsion engine relates the performances of the gas turbine to the thermal efficiency and fuel consumption. The objective of this research is to improve the speed of vessel up to 35 knots with minimum fuel consumption. From the result of this study, the gas turbine is a practical system recommended to install into ecotourism vessel. The recommended gas turbine to be installed lay in the power output ranging 6890hp to 6900 hp.

Acknowledgement: The author thanks Mr. Ong See Ha for his direct contribution to this research

## 4. REFERENCES

1. Boyce, M.P., (2001) “Cogeneration and combined Cycle Power Plant”, Chapter 1, ASME Press, NY

2. Boyce M.P Meherwan., P.Boyce, Phd, Pe. “Cogeneration and Combined Cycle Power Plant”, Chapter 1, Gas turbine (third edition)

3. Yousef S.Najjar., “Enchancement of performances of gas turbine engines by inlet air

4. Farmer.R., “Design 60% Net Efficiency in Frame 7/9H Steam Cooled CCGT” Gas turbine World,May-June 1995

5. Gas turbine (third edition) Engineering Handbook, Meherwan P.Boyce, Phd. And Pe

6. Roy L. Harrigton. , “Marine Engineering”, Engineering Technical Department, New port News shipbuilding and Dry Dock Company

7. Roberto Carapellucci. , Adriano Milazzo, “Thermodynamic optimiation of the reheat chemically recuparated gas turbine” Department of Engineering University of L’Aquila, Italy

8. Yunus A cengel. , “Thermodynamic an engineering approach six edition”, University of Nevada, Reno, Michael A.Boles, University of north Carolins

9. O.Sulaiamn et al. “Potential of Biomass cogereation for Marne System Powering, Bioscience, Biotechnology Journal, Vol (7) 2, 2010

10. Blake,J.W and R.W.Tumy., (1950), “ Huey Gas Turbine Ticks Off 3400 Hours.”Powe, Vol. 94, February, pp96-102

11. C.B Barras (2004)., “ Ship Design and Performance for Master and Mates .” Elsevier’s Science and Technology. Oxford: 55-81

12. Parks WP., Jr,Hoffman P., Karnitz MA., Wright IG. “The advance gas turbine systems program in the USA.”

13. J,Schubert F,Ennis PJ,editor.Materials for advanced power engineering, Forschungszentum Julich; pp 1789-1805

14. I.G.wright and T.B.Gribbons.,(2006) “Recent Development in Gas Turbine and Technology and Their implication forSyngas Firing” Material Sciences and Technology Division, Oak Ridge National Laboratory, USA; 3612-3619

15. William D. Callister., Material Science and Engineering: an Introduction. Deparment of Metallurgical Engineering,The University of Utah: 743, 838-860

# Abrasive Wear of Digger Tooth Steel

**Hussein Sarhan** sarhan_52@hotmail.com
*Faculty of Engineering Technology, Department of Mechatronics Engineering, Al-Balqa' Applied University, Amman, PO Box: 15008, Jordan*

**Nofal Al-Araji** nofalaraji@yahoo.uk.com
*Faculty of Engineering, Department of Materials and Metallurgical Engineering, Al-Balqa' Applied University, Al-Salt, Jordan*

**Rateb Issa** ratebissa@yahoo.com
*Faculty of Engineering Technology, Department of Mechatronics Engineering, Al-Balqa' Applied University, Amman, PO Box: 15008, Jordan*

**Mohammad Alia** makalalia2000@yahoo.com
*Faculty of Engineering Technology, Department of Mechatronics Engineering, Al-Balqa' Applied University, Amman, PO Box: 15008, Jordan*

**Abstract**

The influence of silicon carbide SiC abrasive particles of 20, 30, 40, 50 and 60 $\mu m$ size on carburized digger tooth steel was studied. Four types of steel, with different hardness, were tested at two constant linear sliding speeds and under various loads of 10, 20, 30, 40 and 50N. Tests were carried out for sliding time of 0.5, 1.0, 1.5, 2.0 and 2.5min. Experimental results showed that there was consistent reduction in abrasive wear as the hardness of the materials was increased. It was found that wear increased with the increase of applied load, linear sliding speed and sliding time. Also, it was noticed that the wear increased with increase in abrasive particle size, and the most effective size was 40 $\mu m$. SEM observations of the worm surface showed that the cutting and ploughing were the dominant abrasive wear mechanisms.

**Keywords:** Abrasive Wear, Wear Resistance, Carburized Digger Tooth Steel.

## 1. INTRODUCTION

Wear processes in metals have been classified into many types depending on the mechanism responsible for removal of material from the surface. Experiments have revealed that wear is a very complex process. Wear predictions, even through flawed, can be used in a number of ways besides estimating the wear rate. First, an equation for wear indicates the relative influence of various parameters, such as load, hardness, linear sliding speed, and surface roughness that

suggest changes in wear that might result, if the sliding system is changed. Second, component of the wear is also important in the failure analysis or in the study of any worn component of a system. Quantitative analysis of wear starts with the concept that while a sliding system may be loosing material in more than one way, another mechanism will dominate the overall wear rate [1].

The failure of components in service can be often attributed to wear, erosion or corrosion-enhanced wear and erosion. The phenomenon contributing to failure under all these conditions is complex and often specific to the particular application. Material properties determining resistance to wear and erosion are correspondingly complex, making it difficult to predict the service behavior of a particular material. Generally, high hardness, rapid work hardening, and good oxidation and corrosion resistance can all contribute to wear and erosion resistance. Common materials currently used in sever wear and erosion applications include cobalt-based alloys, high manganese stainless steels, and other chromium containing alloys [2]. Under different testing conditions, all results showed that there was a decreasing trend in wear with increasing hardness of hard metals [3]. In experiments testing wear mechanisms, once equilibrium surface conditions have been established, the wear rate is normally independent of the area of contact. The wear rate is therefore proportional to the load for only a small numbers of variations, but there is still a small deviation between wear rate and load that forms a direct proportionality. Published literatures concluded that wear rate is proportional to the load and independent of pressure unless the area of contact was equivalent to one third of materials' hardness [4]. The most widely used quantitative relationship among abrasive wear rate, material properties, load and sliding speed, at the interface of two bodies loaded against each other in relative motion, was formulated [5]. Also, it was reported that wear rates of some materials vary linearly with the applied load and independent of pressure over a wide range. It was shown that there is an inverse relationship between wear rates and hardness. Wear is quantified by weight or volume loss per unit of time or per sliding distance. These simple results are marked in contrast to the majority of wear experiments reported in literature. They suggest that wear is dependent on a large number of variables and there is no general agreement about how the wear depends on such variables as applied load, linear sliding speed, and apparent area of contact. Generally, the abrasive wear of alloy steel is characterized by two modes, designated sever wear and mild wear. This has been recognized by many investigators for a long time [6]. It has been found that, at the constant linear sliding speed used, in the load range, where equilibrium mild wear operates, the sliding distance for initiation of mild wear decreases logarithmically with the load. The slope of this decrement is termed the running-in coefficient and is a quantitative measure of the running-in behavior of the steel. The presence of 3% Cr markedly decreases the running-in coefficient, i.e. increases the sliding distance required for the initiation of mild wear at a given load [7].

Hard metals could be an ideal solution for wear resistance. At present, hardened steel or some technical ceramic materials, in bulk or as a surface coating, are often used. The main purpose of these materials is to extend the life time of existing devices and/ or components by decreasing their wear rate. A significant disadvantage of these materials is their relatively high friction coefficient in dry contact conditions (heat development and energy loss). Moreover, their high hardness renders them intrinsically difficult to shape and to finish using conventional methods [8]. High chromium content white cast irons have generally good wear resistance and toughness properties. These types of cast irons are generally used in slurry pumps, brick dies, and several mine drilling equipment. Rock chromium content cast iron materials have higher toughness than have low chromium ones [9]. Investigations of the wear behavior of white cast irons under different compositions were conducted against SiC and $Al_2O_3$ abrasive paper, and the results showed that the wear rate was affected by the composition of white cast iron [10]. White cast iron containing copper under erosive wear testing has been devised, and the results showed that a linear relationship has been established between the percentage of copper and the amount of erosion. Relative erosion is directly dependent on the carbide volume, carbide particle size and also the angle of impact [7]. The results of wear test of hard boron carbide $B_4C$ thin films, and the data obtained from pin-on-disc tests show that the abrasiveness of a contact is proportional to the number of asperities in the contact and the effect of increasing the load is to enlarge the initial

apparent contact region, and the dependence of the wear rate on load follows relationships that are similar to Hertzain relationships [11].

The aim of this work is to investigate the role of abrasive particles size and other factors on the wear properties of carburized digger tooth steel. There are a number of different types of wear testing methods. Low stress or scratching abrasion is probably the most predominate in the mining industry. A quantitative method of measuring a materials resistance to this scratching type abrasion is the pin-on-disc apparatus, (ASTM G99-05, 2006). This test characterizes materials removed in terms of weight loss under a controlled set of laboratory conditions. Correlation to actual field conditions which may be influenced by other wear parameters, such as the amount of impact, corrosion, galling, etc. is required.

## 2. EXPERIMENTAL WORK

Pins of 8mm diameter and 80mm length for wear test were prepared by machining them from digger tooth steel. The composition of the digger tooth steel used for this study is listed in Table 1. All pins were case hardened under pack carburizing conditions given in Table 2.

| C% | Si% | Mn% | Mo% | Ni% | Al% | P% | S% | HRC |
|---|---|---|---|---|---|---|---|---|
| 0.40-0.42 | 0.40 | 0.90-0.95 | 0.25 | 0.20 | 0.04 | 0.03 | 0.02 | 45 |

**TABLE 1:** Composition of the Digger Tooth Steel.

| Group No. | Holding time, h | Cooling medium | Heating temperature, $^{o}$C | HRC |
|---|---|---|---|---|
| 1 | 16 | Air | 980 | 64 |
| 2 | 12 | Air | 850 | 58 |
| 3 | 10 | Air | 750 | 52 |

**TABLE 2:** Carburizing Conditions of Test Pins.

The carburized pins were heated to 850$^{o}$C for 30min then water-hardened. Abrasive wear tests were carried out at room temperature on a pin-on-disc apparatus shown in Figure 1. The steel disc, $\varphi$ 230mm, was covered with abrasive papers of different SiC particles size of 20-30-40-50-60 $\mu$m. Pins were pressed on the disc with different normal loads of 10-20-30-40-50N. Wear data were collected after 0.5, 1.0, 1.5, 2.0, and 2.5min. Wear tests were carried out at two different linear sliding speeds of 1.5 and 2.5m/s. Abrasive wear was determined from the change in the weight using $1.00 \times 10^{-4}$g precision digital scale. For each wear test a new pin has been used in a new sliding position. Microscopic views of the test pins were taken, also worn surfaces of pins were examined using scanning electron microscope.

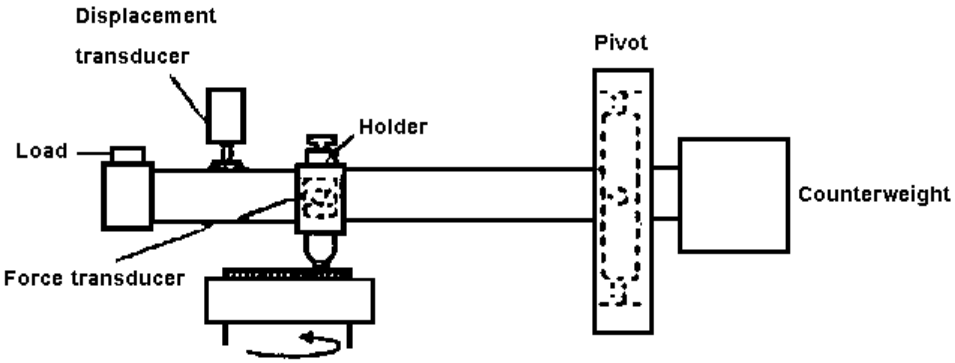


**FIGURE 1:** Schematic Diagram of a Typical Pin-on-Disc Tester.

## 3. RESULTS AND DISCUSSIONS

### Effect of Sliding Time On The Total Weight Loss

The relationship between total weight loss TWL and sliding time for the specimens used in the tests is shown in Figures 2-6. The specimens used in these tests were all subjected to the same load (10N), linear sliding speed (1.5m/s), and abraded against SiC papers with different particle size (20-60 μm). These plots showed that the total weight loss increased as the sliding time increased. This increase in total weight loss was sharper until sliding time of 2.0min, and then the relationship behaved as steady state, especially for the SiC particles size of 50-60 μm. This trend may be due to the increase in temperature of the worn surface and the work hardening effects. Thus, the specimen hardened to 64HRC will exhibit better wear resistance comparing with the same specimen hardened to 45HRC [12].

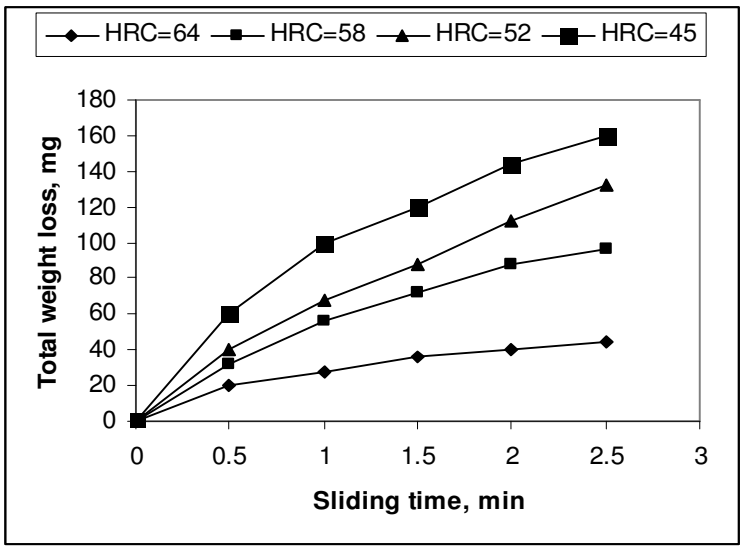


**FIGURE 2:** Effect of Sliding Time on the Total Weight Loss for Load = 10 N, Linear Sliding Speed = 1.5 m /s and SiC Particles Size = 20 μm.

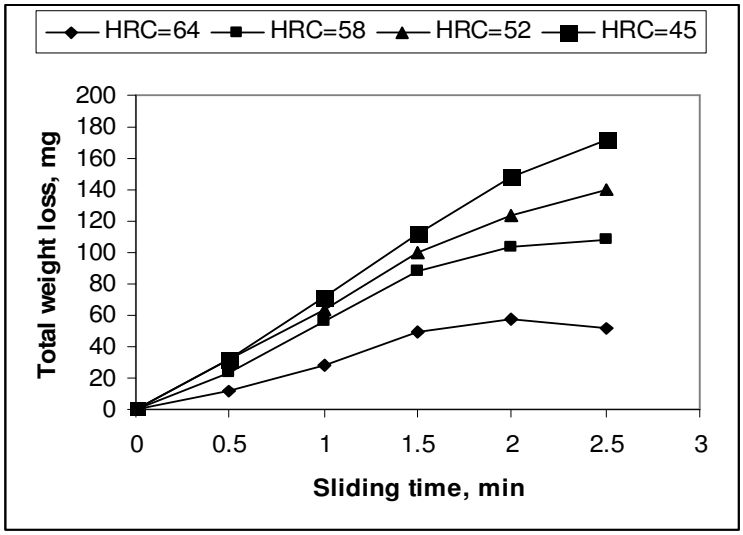


**FIGURE 3:** Effect of Sliding Time on the Total Weight Loss for Load = 10 N, Linear Sliding Speed = 1.5 m /s and SiC Particles Size = 30 μ m.

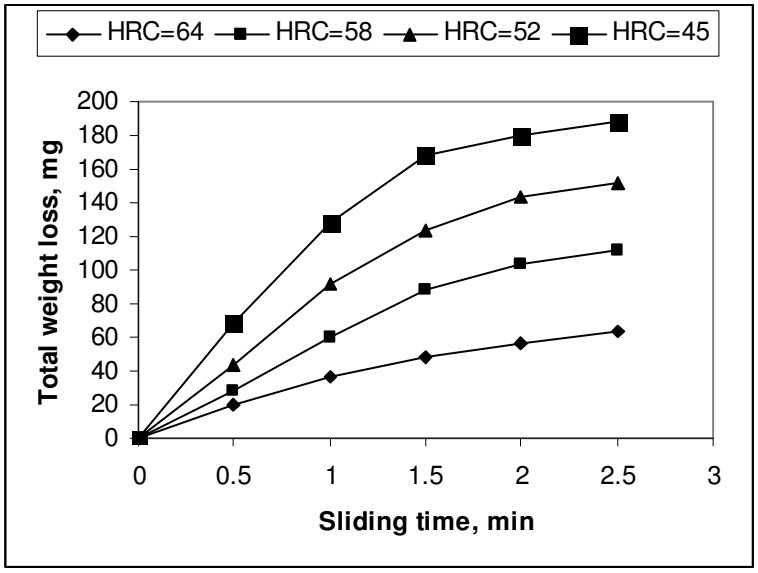


**FIGURE 4:** Effect of Sliding Time on the Total Weight Loss for Load = 10 N, Linear Sliding Speed = 1.5m /s and SiC Particles Size = 40 μ m.

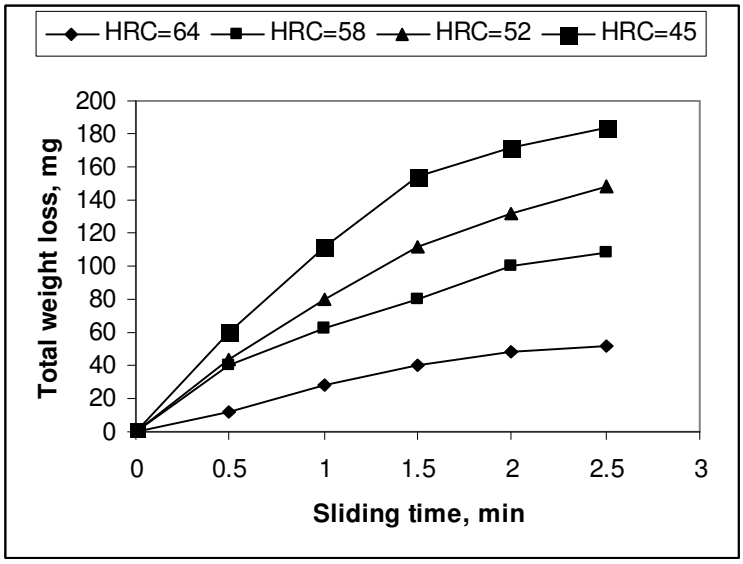


**FIGURE 5:** Effect of Sliding Time on the Total Weight Loss for Load = 10 N, Linear Sliding Speed = 1.5m /s and SiC Particles Size = 50 μ m.

**Effect Of Abrasive Articles Size On The Total Weight Loss**

This means that the specimen with 64HRC is more abrasive wear resistant than that with the total weight loss for four specimens with different hardness as a function of SiC particles size is shown in Figure 6. The specimens were subjected to the same load (10N), sliding speed (1.5m/s), and abraded against SiC papers with different particles size (20-60 μ m) for 2.5min sliding time.

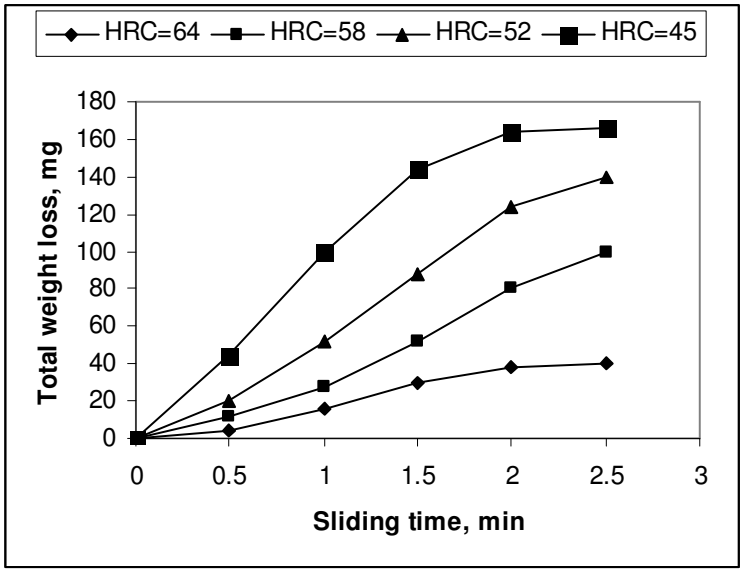


**FIGURE 6:** Effect of Sliding Time on the Total Weight Loss for Load = 10 N, Linear Sliding Speed = 1.5 m/s and SiC Particles Size = 60 μ m.

Figure 7 shows that the specimen with 45HRC is the most worn one, while the specimen with 60HRC is the least worn one, and the total weight loss has been increased with increasing in SiC particles size. It is considered that the total weight loss for all specimens is maximum when they are abraded by SiC of 40 μ m size, which is the critical size, and then the effect of SiC particles

size has been decreased due to the change in their mechanical action from cutting to scratching and deformation [13].

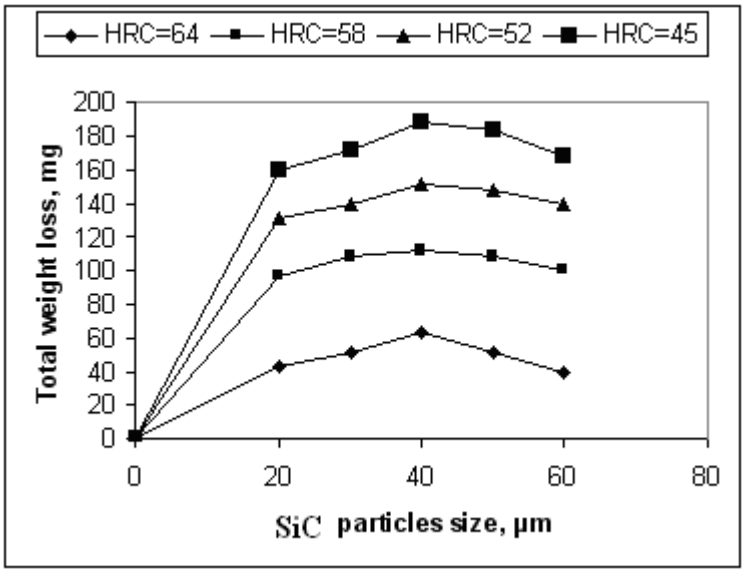


**FIGURE 7:** Effect of SiC Particles Size on the Total Weight Loss for Load = 10 N, Linear Sliding Speed = 1.5m/s and Sliding Time = 2.5 min.

Figures 8 and 9 show the worn surfaces of the specimens of 64HRC abraded under the same abrasive wear conditions (load =10N, sliding speed=1.5m/s and sliding time=2.5min).

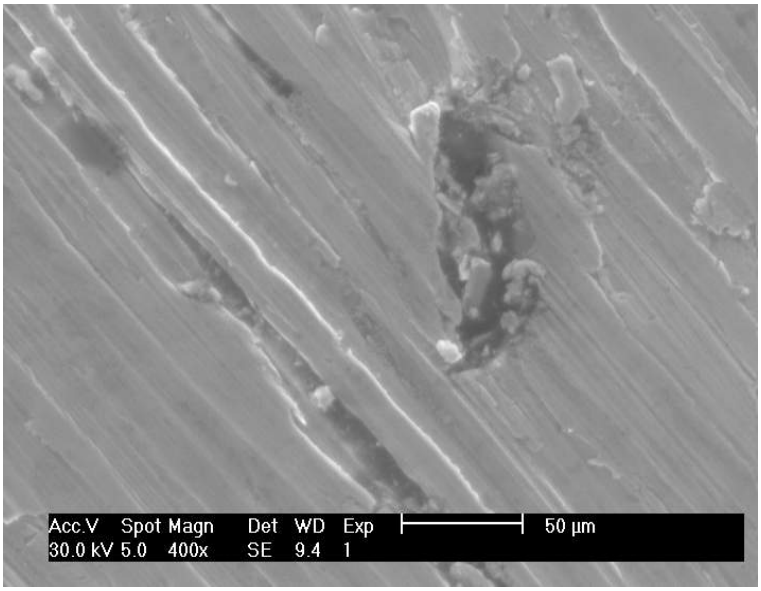


**FIGURE 8:** SEM Micrograph of Worn Surface of 64HRC Specimen Exposed to Abrasive Wear with 40 µm SiC.

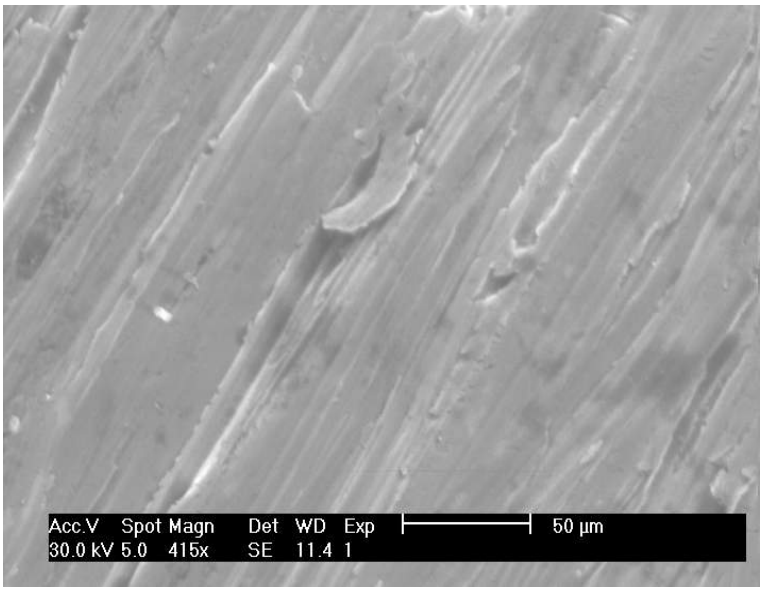


**FIGURE 9:** SEM Micrograph of Worn Surface of 64HRC Specimen Exposed to Abrasive Wear with 60 µm SiC.

Figures 10 and 11 show the SEM micrographs of worn surfaces of digger tooth steel before case hardening (45HRC) and after case hardening (64HRC) abraded under the same abrasive wear conditions (applied load =50N, linear sliding speed =2.5m/s, and sliding time =2.5min). It is clear from Figs. 10 and 11 that the surface damage before case hardening is more than that after case hardening45HRC.

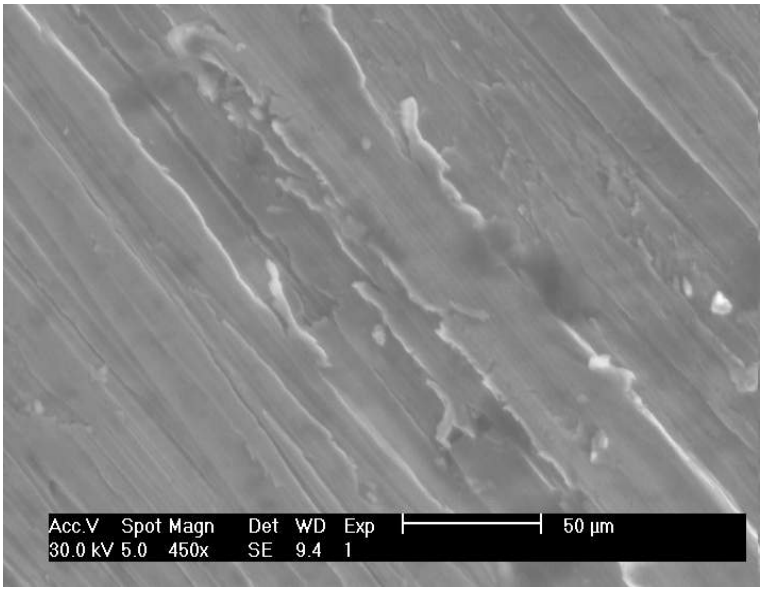


**FIGURE10:** SEM Micrograph of Worn Surface of 45 HRC Specimen Exposed to Abrasive Wear with 40 µm SiC Particles, 50 N load, and 2.5m/s Linear Sliding Speed.

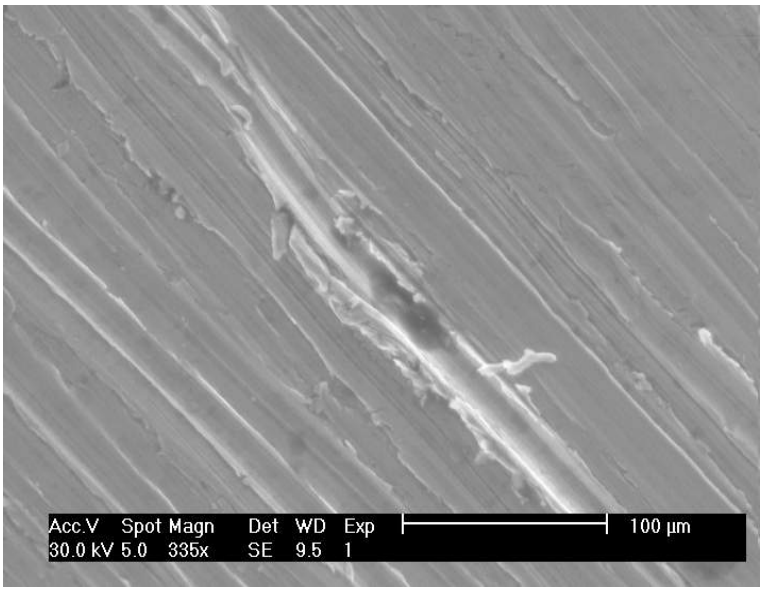


**FIGURE11:** SEM Micrograph of Worn Surface of 64 HRC Specimen Exposed to Abrasive Wear with 40 µm SiC Particles, 50 N Load, and 2.5m/s Linear Sliding Speed.

**Effect Of Load On The Total Weight Loss**

The total weight loss of the specimens as a function of applied load after 2.5min sliding time with 1.5-2.5m/s sliding speed and SiC particles size of 40 µm is shown in Figures 12 and 13. The plots on the mentioned figures show that the total weight loss for all specimens has been increased with increasing the applied load at constant linear sliding speed. Also, the plots show that the total weight loss has been increased with increasing the linear sliding speed under constant test conditions. Transition curve has been obtained for each specimen. The transition curves show three distinct regions: mild wear, transitional wear indicating a possible change in wear mechanism, and sever wear. These regions become clearer as the HRC of the specimens increases. The transitional wear region occurs between 20-40N loads for 1.5m/s linear sliding speed, and 20-30N loads for 2.5m/s linear sliding speed. This trend is related to the temperature effect at the worn surface [3].

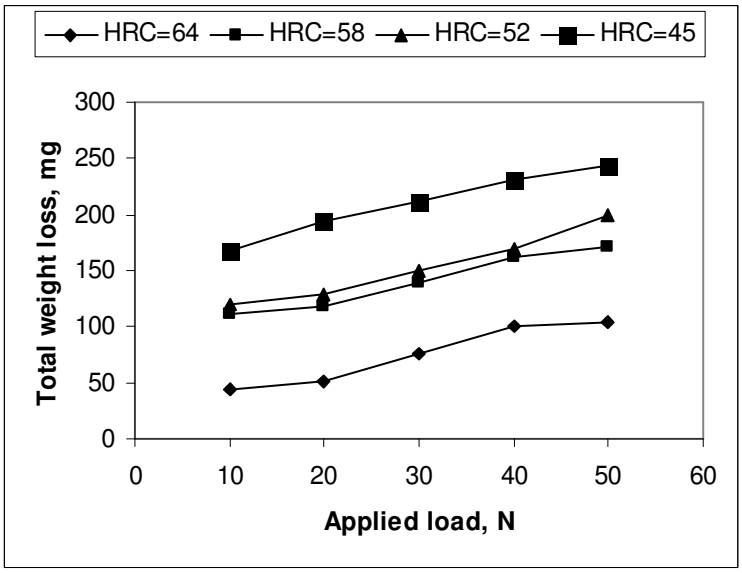


**FIGURE 12:** Effect of Applied Load on the Total Weight Loss under Sliding Speed =1.5m /s, Sliding Time =2.5 min and SiC Particles size =40 μ m.

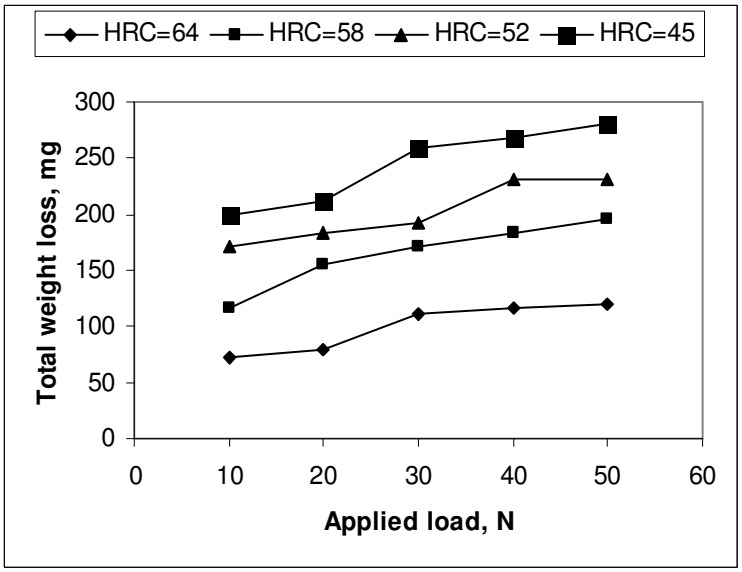


**FIGURE 13:** Effect of Applied Load on the Total Weight Loss under Sliding Speed =2.5m/s, Sliding Time =2.5min, and SiC Particles Size =40 μ m.

**Effect Of Specimens Hardness On The Total Weight Loss**

As mentioned earlier, wear depends on a number of parameters including material hardness. The specimens used in wear tests were all subjected to the same test conditions, but due to their individual hardness, some of them, such as specimen with 64HRC, were more resistant to wear than others [11]. Figure 14 shows a trend for decreasing wear with increasing specimens' hardness and the wear in specimen of 45 HRC is twice greater than the wear in specimen of 64 HRC. The microstructure of heat treated test specimens before case hardening is shown in Figure 15. Concerning Figure 16, it shows the optical microscope photograph of steel carburized 16h to surface carbon content 0.9%, while Figure 17 shows the optical microscope photograph of water-hardening steel-case hardness was 64HRC and core hardness was 45HRC. Figures 16

and 17 show the appearance of carbide layer on the surface, which increases the hardness, and as a result, the abrasive wear has been reduced comparing with the digger tooth steel microstructure shown in Figure 15, before case hardening.

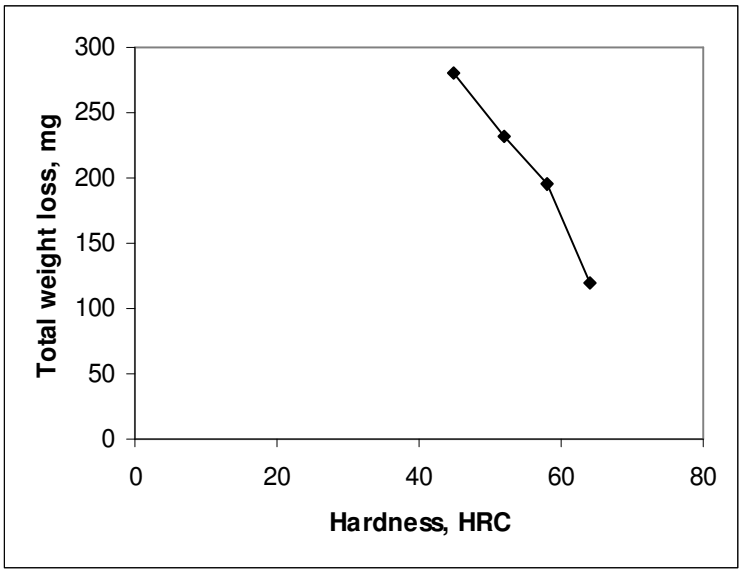


**FIGURE 14:** Effect of Hardness on the Total Weight Loss under Applied Load =50N, Sliding Time =2.5min, Linear Sliding Speed =2.5m/s, and SiC Particles Size = 40 μ m.

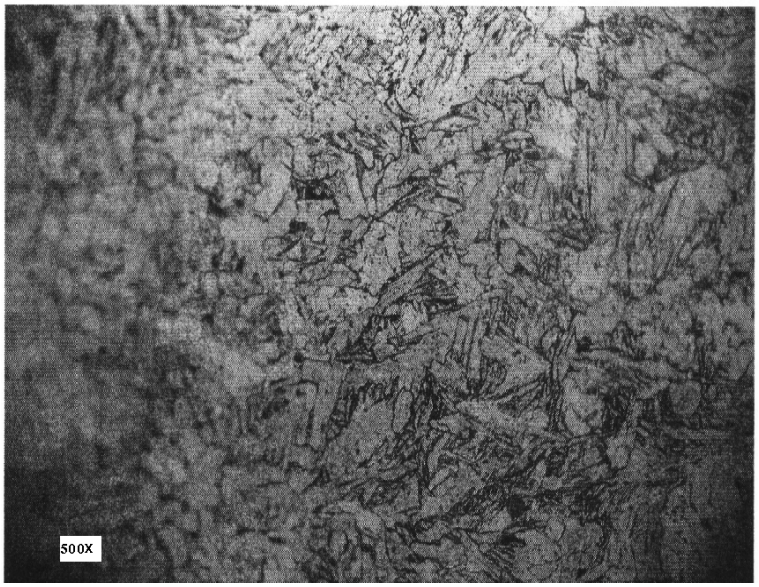


**FIGURE15:** Optical Microscope Photograph of Heat Treated Digger Tooth Steel before Case Hardening Showing Fine Grain of Ferrite and Pearlite.

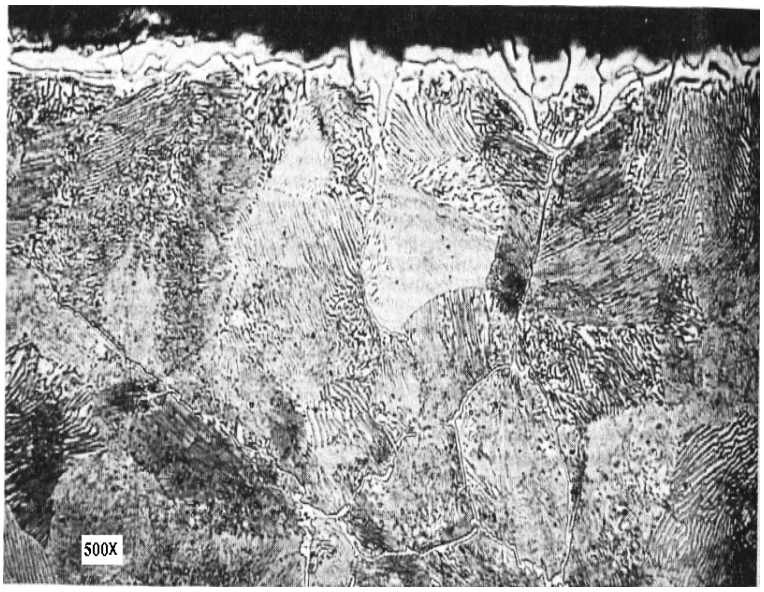


**FIGURE16:** Optical Microscope Photograph of Steel Carburized 16h to a Surface Carbon Content 0.9% Showing Carbide Surface Layer.

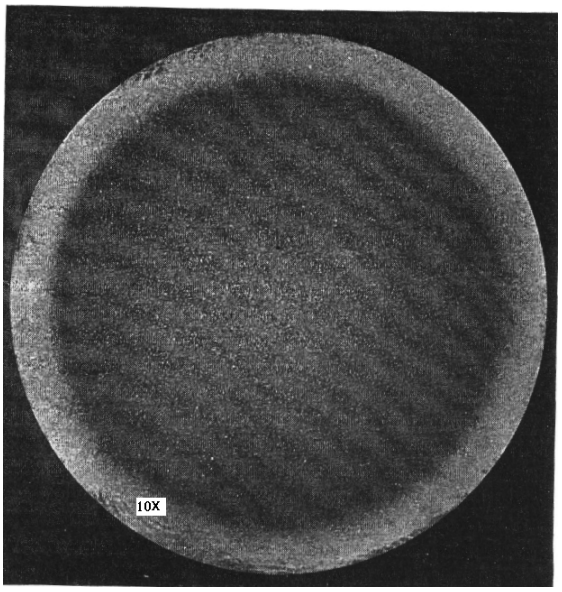


**FIGURE 17:** Optical Microscope Photograph of Water-Hardening Steel. Case Hardness = 64HRC; Core Hardness=45HRC Showing Light Gray Martensitic Zone.

**Effect Of Linear Sliding Speed On The Total Weight Loss**

Figures 12 and 13 show the effect of linear sliding speed on the total weight loss. The total weight loss in all specimens abraded under the same abrasive conditions increased as the linear sliding speed increased from 1.5m/s to 2.5m/s. This is due to the increase of the contact surfaces temperature, which leads to softening of the worn surface.

## 4. CONSLUSION

Based on the results of this study, the following conclusions can be made:
1. The total weight loss increases with increase of abrasive particles size, and the maximum wear occurs with a critical abrasive particles size of 40 μm.
2. There is a significant reduction in wear as the hardness of materials increases.
3. Abrasion resistance of materials depends at the same time on a number of factors, such as their hardness, microstructure, applied load, sliding time, sliding speed, and other wear test conditions.
4. The total weight loss increases as the exposed time to abrasive surface, linear sliding speed, and applied load increases.
5. The transitional wear region decreases as the linear sliding speed increases.
6. As the hardness of abraded materials increases the three types of wear regions (mild, transitional, and sever) become more distinct.
7. Examination of worn surfaces shows that ploughing, cutting, and fracture are the dominant abrasive wear mechanism.

## 5. REFERENCES

1. Carrie K. Harris, Justin P. Broussard and Jerry K. Keska. *"Determination of Wear in a Tribo-system".* In Proceedings of the ASEE Gulf-South Western Annual Conference, 2002

2. Carima Sharma, M. Sundararaman, N. Prabhu and G.L. Goswami. "*Bull. Mater. Sci.*", vol. 26, No. 3, Indian Academy of Sciences, 311-314, India, 2003

3. M.G. Gee, A.J. Gant. "*CMMT (MN) 046 Rotating Wheel Abrasion Tests on Hard Metals and Ceramics*". National Physical Laboratory, 20:170-190, UK, May 1999

4. J.F. Archard, W. Hirst. "*The Wear of Materials under Unlubricated Conditions*". In Proce. Royal Soc., A-236: 71-73, June 1958

5. ASTM. *"Standard Test Method for Wear Testing with a Pin-on-Disc Apparatus*". May 2000

6. Q.M. Farrell, T.S. Eyre. "*The Relationship between Load and Sliding Speed Distance in the Initiation of Mild Wear in Steels*". Wear, 15: 359-372, March 1970

7. F.M. Borodich et al. "*Wear and Abrasiveness of Hard Carbon-Containing Coatings under Variation of the Load*". Surface and Coatings Technology, 179:78-82, 2004

8. A.G. Evans, D.B. Marschall and D.A. Rigney. "*Fundamentals of Friction and Wear of Materials".* ASM, p. 439, 1981

9. "*Metals Handbook*", 9th ed. 15 Casting, (1988)

10. N. Al-Araji. "*Erosion Resistance of White Cast Iron*". Journal of Engineering and Technology, 34: 70-80, University of Technology, Baghdad, Iraq, 1984

11. *"Timken Latrobe Steel, Wear Resistance of Tool Steels*", Marlborough, MA, (2002)

12. N. Al-Araji, H. Sarhan. "*Abrasive Wear of Al-Mn Alloys*", Dirasat, Engineering Sciences, 32(1): 68-77, Jordan University, 2005

13. Cetinkaya. *"An Investigation of the Wear Behaviors of White Cast Irons under Different Compositions*". Material and Design, 2004.

# Prediction the Biodynamic Response of the Seated Human Body using Artificial Intelligence Technique

**Mostafa A. M. Abdeen** mostafa_a_m_abdeen@hotmail.com
*Faculty of Engineering/Dept. of Engineering Mathematics and Physics*
*Cairo University*
*Giza, 12211, Egypt*

**W. Abbas** Wael_abass@hotmail.com
*Eng. Physics and Mathematics Dept.,*
*Faculty of Eng. (Mataria)*
*Helwan University*
*Cairo, Egypt*

**Abstract**

The biodynamic response behaviors of seated human body subject to whole-body vibration have been widely investigated. The biodynamic response characteristics of seated human subjects have been extensively reported in terms of apparent mass and driving-point mechanical impedance while seat-to-head vibration transmissibility has been widely used to characterize response behavior of the seated subjects exposed to vibration. These functions (apparent mass, driving-point mechanical impedance) describe “to-the-body” force–motion relationship at the human–seat interface, while the transmissibility function describes “through-the-body” vibration transmission properties. The current study proposed a 4-DOF analytic biomechanical model of the human body in a sitting posture without backrest in vertical vibration direction to investigate the biodynamic responses of different masses and stiffness. Following the analytical approach, numerical technique developed in the present paper to facilitate and rapid the analysis. The numerical analysis used here applies one of the artificial intelligence technique to simulate and predict the response behaviors of seated human body for different masses and stiffness without the need to go through the analytic solution every time. The Artificial Neural Network (ANN) technique is introduced in the current study to predict the response behaviors for different masses and stiffness rather than those used in the analytic solution. The results of the numerical study showed that the ANN method with less effort was very efficiently capable of simulating and predicting the response behaviors of seated human body subject to whole-body vibration.

**Keywords:** Biodynamic Response, Analytic Seated Human Body Model, Numerical Simulation Model, Artificial Neural Network.

## 1. INTRODUCTION

The biodynamic responses of seated human occupant exposed to vibration have been widely characterized to define frequency-weightings for assessment of exposure, to identify human

sensitivity and perception of vibration, and to develop seated body models [1]. The biodynamic response of the human body exposed to vibration have been invariably characterized through measurement of force motion relationship at the point of entry of vibration "To-the-body response function", expressed as the driving-point mechanical impedance (DPMI) or the apparent mass (APMS) and transmission of vibration to different body segments "Through-the-body response function", generally termed as seat-to-head transmissibility (STHT) for the seated occupant. Considering that the human body is a complex biological system, the "To-the-body" response function is conveniently characterized through non–invasive measurements at the driving point alone.

The vast majority of the reported studies on biodynamic response to whole-body vibration have considered vibration along the vertical axis alone. In many of the early studied, such as those conducted by Coermann [2], Vogt [3], and Suggs [4], the numbers of subjects was usually relatively small, and only sinusoidal excitation was used, not generally representative of the type of excitation and levels of vibration usually encountered in practice. In many of these studies, the feet of the subjects were either not supported or supported but not vibrated, a condition not common in most driving situations. Fairley and Griffin [5], reported the vertical apparent mass of 60 seated subjects including men, women and children, which revealed a large scatter of data presumably owing to large variations in the subject masses. Boileau et al. [6] investigated the relationships between driving point mechanical impedance and seat-to-head transmissibility functions based upon 11 reported one dimensional lumped parameter models. The majority of the models showed differences in frequencies corresponding to peak magnitudes of the two functions, which were expressed as resonant frequencies. Toward [7], summarized that a support of the back caused higher resonance frequency and slightly lower peak magnitude of the APMS response for subjects sitting on a horizontal plane. Wang et al. [8], study the vertical apparent mass and seat-to-head transmissibility response characteristics of seated subjects are derived through measurements of total biodynamic force at the seat pan, and motions of the seat pan and head along the applied input acceleration direction, using 12 male subjects. The data were acquired under three different back support conditions and two different hands positions representative of drivers and passengers-like postures. Steina et al.[9], analyzed apparent mass measurements in the y- direction with a group of 13 male test subjects exposed to three excitation intensities.

In early studies, various biodynamic models have been developed to depict human motion from single-DOF to multi-DOF models. These models can be divided as distributed (finite element) models, lumped parameter models and multi-body models. The distributed model treats the spine as a layered structure of rigid elements, representing the vertebral bodies, and deformable elements representing the intervertebral discs by the finite element method. Multi-body human models are made of several rigid bodies interconnected by pin (two-dimensional) or ball and socket (three-dimensional) joints, and can be further separated into kinetic and kinematic models. It is clear that the lumped-parameter model is probably one of the most popular analytical methods in the study of biodynamic responses of seated human subjects, though it is limited to one-directional analysis. However, vertical vibration exposure of the driver is our main concern. Therefore, this paper carries out a thorough survey of literature on the lumped- parameter models for seated human subjects exposed to vertical vibration.

The lumped parameter models consider the human body as several rigid bodies and spring-dampers. This type of model is simple to analyze and easy to validate with experiments. However, the disadvantage is the limitation to one-directional analysis. Coermann [2], measured the driving-point impedance of the human body and suggested 1-DOF model. Suggs et al. [4], developed a 2-DOF human body. It was modeled as a damped spring-mass system to build a standardized vehicle seat testing procedure. A 3-DOF analytical model for a tractor seat suspension system is presented by Tewari et al. [10]. It was observed that the model could be employed as a tool in selection of optimal suspension parameters for any other type of vehicles. Boileau et al. [11] used an optimization procedure to establish a 4-DOF human model based on test data. It is quite clear from the literature mentioned previously the amount of effort

(experimentally or analytically) required to accurately investigate and understand the biodynamic response behaviors of seated human body subject to whole-body vibration of different types and magnitudes. This fact urged the need for utilizing new technology and techniques to facilitate this comprehensive effort and at the same time preserving high accuracy.

Artificial intelligence has proven its capability in simulating and predicting the behavior of the different physical phenomena in most of the engineering fields. Artificial Neural Network (ANN) is one of the artificial intelligence techniques that have been incorporated in various scientific disciplines. Ramanitharan and Li [12] utilized ANN with back-propagation algorithm for modeling ocean curves that were presented by wave height and period. Abdeen [13] developed neural network model for predicting flow depths and average flow velocities along the channel reach when the geometrical properties of the channel cross sections were measured or vice versa. Allam [14] used the artificial intelligence technique to predict the effect of tunnel construction on nearby buildings which is the main factor in choosing the tunnel route. Allam, in her thesis, predicted the maximum and minimum differential settlement necessary precautionary measures. Azmathullah et al. [15] presented a study for estimating the scour characteristics downstream of a ski-jump bucket using Neural Networks (NN). Abdeen [16] presented a study for the development of ANN models to simulate flow behavior in open channel infested by submerged aquatic weeds. Mohamed [17] proposed an artificial neural network for the selection of optimal lateral load-resisting system for multi-story steel frames. Mohamed, in her master thesis, proposed the neural network to reduce the computing time consumed in the design iterations. Abdeen [18] utilized ANN technique for the development of various models to simulate the impacts of different submerged weeds' densities, different flow discharges, and different distributaries operation scheduling on the water surface profile in an experimental main open channel that supplies water to different distributaries.

## 2. PROBLEM DESCRIPTION

To investigate the biodynamic response behaviors of seated human body subject to whole-body vibration (sinusoidal wave with amplitude 5 $m/s^2$ ), analytical and numerical techniques will be presented in this study. The analytical model and its results will be described in detail in the following sections. The numerical models presented in this study utilized Artificial Neural Network technique (ANN) using the data and the results of the analytical model to understand the biodynamic response behaviors and then can predict the behaviors for different data of the human body without the need to go through the analytical solution.

## 3. ANALYTICAL MODEL

### 3.1 Biomechanical Modeling

The human body in a sitting posture can be modeled as a mechanical system that is composed of several rigid bodies interconnected by springs and dampers. (Boileau, and Rakheja [11]). This model as shown in Fig. 1 consists of four mass segments interconnected by four sets of springs and dampers. The four masses represent the following four body segments: the head and neck ($m_1$), the chest and upper torso ($m_2$), the lower torso ($m_3$), and the thighs and pelvis in contact with the seat ($m_4$). The mass due to lower legs and the feet is not included in this representation, assuming they have negligible contributions to the biodynamic response of the seated body. The stiffness and damping properties of thighs and pelvis are ($k_4$) and ($c_4$), the lower torso are ($k_3$) and ($c_3$), upper torso are ($k_2$) and ($c_2$), and head are ($k_1$) and ($c_1$).

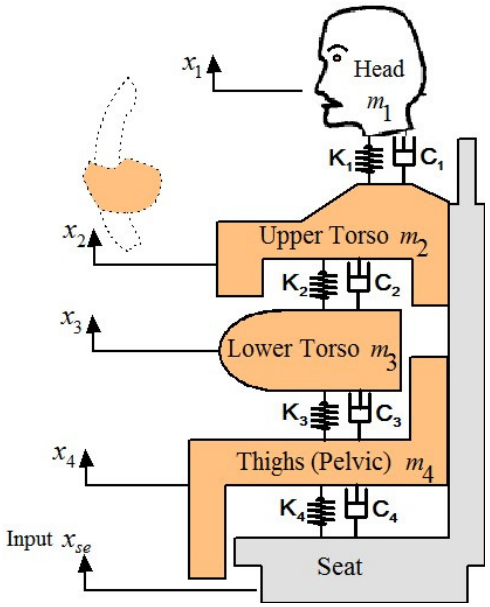


**FIGURE 1:** Biomechanical Boileau and Rakheja 4-DOF model.

The equation of motion of the human body can be obtained as follows:

$$\begin{cases} m_1\ddot{x}_1 = -c_1(\dot{x}_1 - \dot{x}_2) - k_1(x_1 - x_2), \\ m_2\ddot{x}_2 = c_1(\dot{x}_1 - \dot{x}_2) + k_1(x_1 - x_2) \\ \qquad -c_2(\dot{x}_2 - \dot{x}_3) - k_2(x_2 - x_3) \\ m_3\ddot{x}_3 = c_2(\dot{x}_2 - \dot{x}_3) + k_2(x_2 - x_3) \\ \qquad -c_3(\dot{x}_3 - \dot{x}_4) - k_3(x_3 - x_4), \\ m_4\ddot{x}_4 = +c_3(\dot{x}_2 - \dot{x}_4) + k_3(x_2 - x_4) \\ \qquad -c_4(\dot{x}_4 - \dot{x}_{se}) - k_4(x_4 - x_{se}). \end{cases} \tag{1}$$

The system equations of motion, equation (1), for the model can be expressed in matrix form as follows:

$$[\mathrm{M}]\{\ddot{x}\} + [\mathrm{C}]\{\dot{x}\} + [\mathrm{k}]\{x\} = \{f\} \tag{2}$$

where $[\mathrm{M}]$, $[\mathrm{C}]$, and $[\mathrm{k}]$ are $\mathrm{n} \times \mathrm{n}$ mass, damping, and stiffness matrices, respectively; $\{f\}$ is the force vector due to external excitation.

$$[\mathrm{M}] = \begin{bmatrix} m_1 & 0 & 0 & 0 \\ 0 & m_2 & 0 & 0 \\ 0 & 0 & m_3 & 0 \\ 0 & 0 & 0 & m_4 \end{bmatrix},$$

$$[C] = \begin{bmatrix} c_1 & -c_1 & 0 & 0 \\ -c_1 & c_1 + c_2 & -c_2 & 0 \\ 0 & -c_2 & c_2 + c_3 & -c_3 \\ 0 & 0 & -c_3 & c_3 + c_4 \end{bmatrix},$$

$$[\mathrm{k}] = \begin{bmatrix} k_1 & -k_1 & 0 & 0 \\ -k_1 & k_1 + k_2 & -k_2 & 0 \\ 0 & -k_2 & k_2 + k_3 & -k_3 \\ 0 & 0 & -k_3 & k_3 + k_4 \end{bmatrix},$$

And,

$$\{f\} = \begin{Bmatrix} 0 \\ 0 \\ 0 \\ c_4\ \dot{x}_{se} + k_4 x_{se} \end{Bmatrix}.$$

By taking the Fourier transformation of equation (2), the following matrix form of equation can be obtained:

$$\{X(j\omega)\} = [\,[\mathrm{K}] - \omega^2[\mathrm{M}] + j\omega[\mathrm{C}]\,]^{-1}\{F(j\omega)\} \quad (3)$$

where, $\{X(j\omega)\}$ and $\{F(j\omega)\}$ are the complex Fourier transformation vectors of $\{x\}$ and $\{f\}$, respectively. $\omega$ is the excitation frequency. Vector $\{X(j\omega)\}$ contains complex displacement responses of n mass segments as a function of $\omega$ ($\{X_1(j\omega), X_2(j\omega), X_3(j\omega), \ldots, X_n(j\omega)\}$). $\{F(j\omega)\}$ consists of complex excitation forces on the mass segments as a function of $\omega$ as well.

### 3.2 Biodynamic Response of Human Body

The biodynamic response of a seated human body exposed to whole-body vibration can be broadly categorized into two types. The first category "To-the-body" force motion interrelation as a function of frequency at the human-seat interface, expressed as the driving-point mechanical impedance (DPMI) or the apparent mass (APMS). The second category "Through-the-body" response function, generally termed as seat-to-head transmissibility (STHT) for the seated occupant.

The DPMI relates the driving force and resulting velocity response at the driving point (the seat-buttocks interface), and is given by [1]:

$$Z(j\omega) = \frac{F(j\omega)}{V(j\omega)} = \frac{F(j\omega)}{\dot{X}(j\omega)} \quad (4)$$

where, $Z(j\omega)$ is the complex DPMI, $F(j\omega)$ and $V(j\omega)$ or ( $\dot{X}(j\omega)$ ) are the driving force and response velocity at the driving point, respectively. $\omega$ is the angular frequency in rad/s , and $j = \sqrt{-1}$ is the complex phasor.

Accordingly, DPMI for the model can be represented as:

$$\mathrm{DPMI}(j\omega) = \left| \left(c_4 + \frac{k_4}{j\omega}\right)\frac{X_4(j\omega)}{X_0(\omega)} - \left(c_4 + \frac{k_4}{j\omega}\right) \right| \quad (5)$$

In a similar manner, the apparent mass response relates the driving force to the resulting acceleration response, and is given by [19]:

$$\mathrm{APMS}(j\omega) = \frac{F(j\omega)}{a(j\omega)} \quad (6)$$

where, $a(j\omega)$ is the acceleration response at the driving point.

The magnitude of APMS offers a simple physical interpretation as it is equal to the static mass of the human body supported by the seat at very low frequencies, when the human body resembles that of a rigid mass. The above two functions are frequently used interchangeably, due to their direct relationship that given by:

$$APMS(j\omega) = \frac{\mathrm{DPMI}(j\omega)}{j\omega} \tag{7}$$

APMS for the model can be represented as:

$$\mathrm{APMS}(j\omega) = \left| \frac{\mathrm{DPMI}(j\omega)}{j\omega} \right| = \left| \left(\frac{c_4}{j\omega} + \frac{k_4}{-\omega^2}\right)\frac{X_4(j\omega)}{X_0(\omega)} - \left(\frac{c_4}{j\omega} + \frac{k_4}{-\omega^2}\right) \right| \tag{8}$$

The biodynamic response characteristics of seated occupants exposed to whole body vibration can also be expressed in terms of seat-to-head transmissibility (STHT), which is termed as "through-the-body" response function. Unlike the force-motion relationship at the driving-point, the STHT function describes the transmission of vibration through the seated body. The STHT response function is expressed as:

$$H(j\omega) = \frac{a_H\,(j\omega)}{a\,(j\omega)} \tag{9}$$

where, $H(j\omega)$ is the complex STHT, $a_H\,(j\omega)$ is the response acceleration measured at the head of seated occupant, and $a(j\omega)$ is the acceleration response at the driving point. According to equation (9) seat-to-head transmissibility for the model is:

$$\mathrm{STHT}(j\omega) = \frac{X_2(j\omega)}{X_0(\omega)} \tag{10}$$

The above three functions have been widely used to characterize the biodynamic responses of the seated human subjects exposed to whole body vibration.

## 4. ANALYTIC RESULTS AND DISCUSSIONS

On the basis of anthropometric Boileau data [19], the proportion of total body weight estimated for different body segments is 7.5% for the head and neck, 40.2% for the chest and upper torso, 12.2% for the lower torso, and 18.2% for the thighs and upper legs. For a seated driver with mean body mass, maintaining an erect back not supported posture, 78% of the weight was found to be supported by the seat. The biomechanical parameters of the human model (Stiffness, Damping) are listed in Table 1.

| Stiffness Coefficient (N/m) | Damping coefficient (N.s/m) |
|---|---|
| $k_1$ = 310000 | $c_1$ = 400 |
| $k_2$ = 183000 | $c_2$ = 4750 |
| $k_3$ = 162800 | $c_3$ = 4585 |
| $k_4$ = 90000 | $c_4$ = 2064 |

**TABLE 1:** The biomechanical parameters of the Boileau and Rakheja model.

### 4.1 Response Behaviors of the Human Body

In the following subsections the effect of body's mass, stiffness coefficient, and damping coefficient on the response behaviors of the human body (STHT, DPMI, and APMS) will be investigated using the analytical solution presented in the current study.

#### 4.1.1 Effect of Human Body's Mass

Three different total body masses (65, 75, and 85 kg) are used to investigate the effect of mass on the response behaviors of human body (STHT, DPMI and APMS) as shown in Fig. 2 (a, b, and c) respectively. From these figures, one can see that by increasing the human body mass, the biodynamic response characteristics of seated human body (STHT, DPMI, and APMS) are increased.

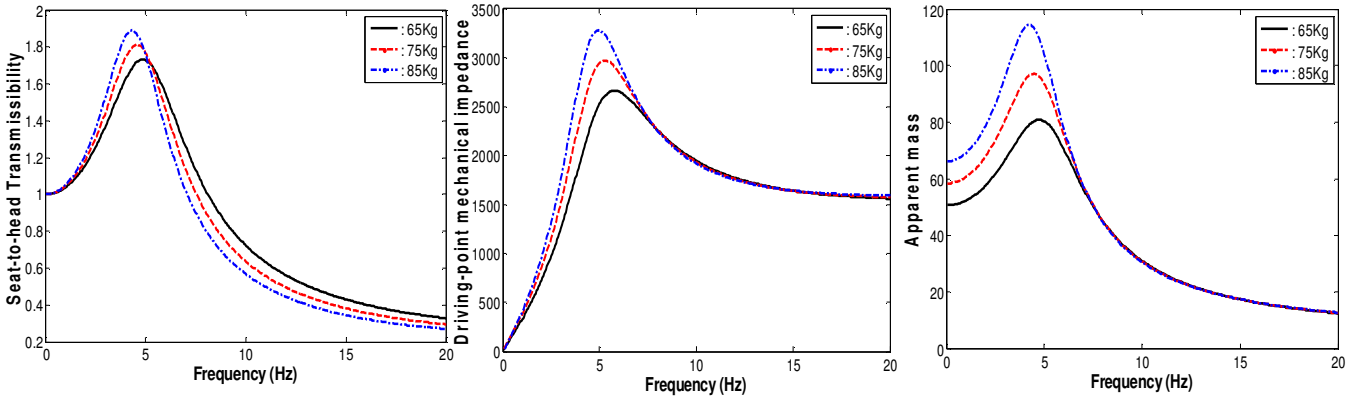


(a) (b) (c)

**FIGURE 2:** Effect of human body's mass on the biodynamic response behavior (Analytic Results)((a) STHT, (b) DPMI and (c) APMS).

### 4.1.2 Effect of Stiffness Coefficient

Three different values of pelvic stiffness $k_4$ (Boileau value (B.V.), B.V. +40%, and B.V. -40%) are used to investigate the effect of pelvic stiffness on the response behaviors of human body (STHT, DPMI and APMS) as shown in Fig. 3 (a, b, and c) respectively. From these figures, it is clear that by increasing the pelvic stiffness, the biodynamic response characteristics of seated human body (STHT, DPMI, and APMS) are increased.

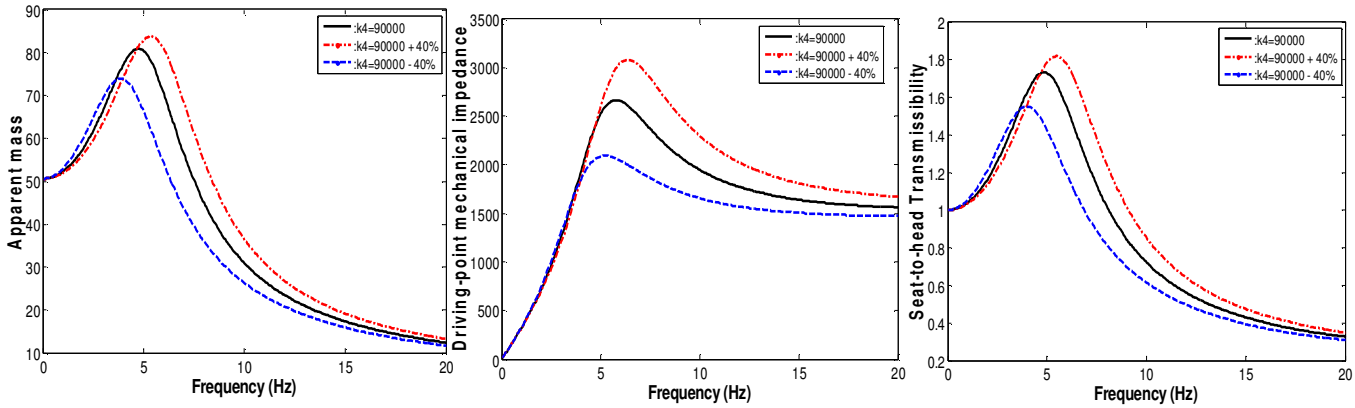


(a) (b) (c)

**FIGURE 3:** Effect of stiffness coefficient on the biodynamic response behaviors (Analytic Results) ((a) STHT, (b) DPMI and (c) APMS).

### 4.1.3 Effect of Damping Coefficient

Three different values of pelvic damping coefficient $C_4$ (Boileau value (B.V.), B.V. +40%, and B.V. -40%) are used to investigate the effect of pelvic damping coefficient on the response behaviors of human body (STHT, DPMI and APMS) as shown in Fig. 4 (a, b, and c) respectively. From these figures, it is clear that by increasing pelvic damping coefficient, the biodynamic response characteristics of seated human body (STHT, DPMI, and APMS) are decreased.

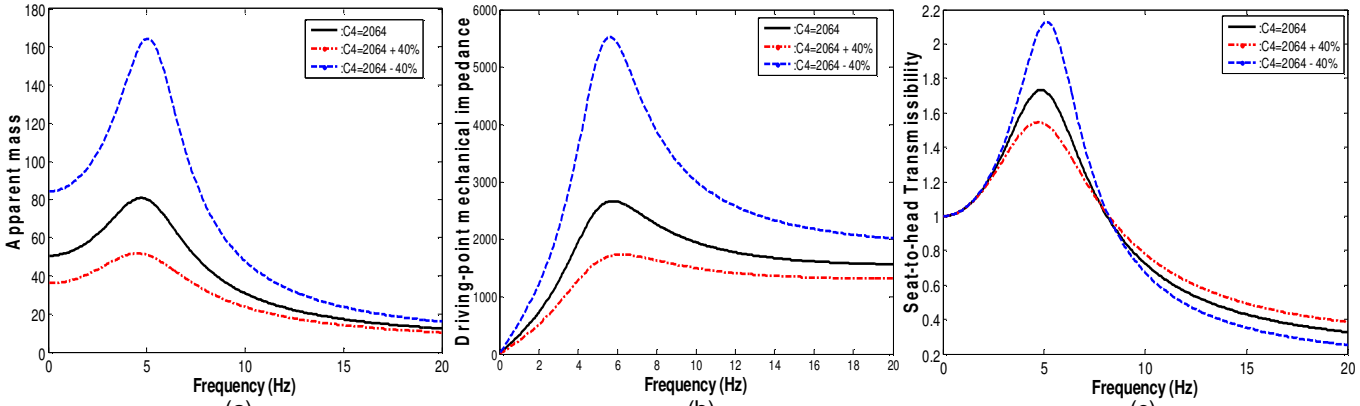


(a) (b) (c)

**FIGURE 4:** Effect of damping coefficient on the biodynamic response behaviors (Analytic Results) ((a) STHT, (b) DPMI and (c) APMS)

## 5. NUMERICAL MODEL STRUCTURE

Neural networks are models of biological neural structures. Abdeen [13] described in a very detailed fashion the structure of any neural network. Briefly, the starting point for most networks is a model neuron as shown in Fig. (5). This neuron is connected to multiple inputs and produces a single output. Each input is modified by a weighting value (w). The neuron will combine these weighted inputs with reference to a threshold value and an activation function, will determine its output. This behavior follows closely the real neurons work of the human's brain. In the network structure, the input layer is considered a distributor of the signals from the external world while hidden layers are considered to be feature detectors of such signals. On the other hand, the output layer is considered as a collector of the features detected and the producer of the response.

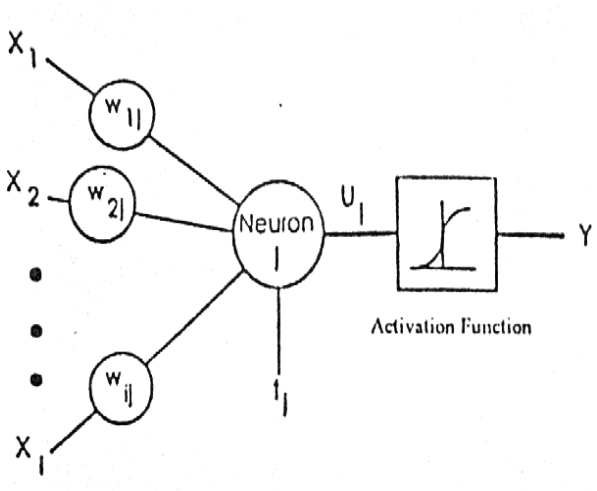


**FIGURE 5:** Typical picture of a model neuron that exists in every neural network

### 5.1 Neural Network Operation

It is quite important for the reader to understand how the neural network operates to simulate different physical problems. The output of each neuron is a function of its inputs ($X_i$). In more details, the output ($Y_j$) of the $j^{th}$ neuron in any layer is described by two sets of equations as follows:

$$U_j = \sum\left( X_i w_{ij} \right) \tag{11}$$

And

$$Y_j = F_{th}\left(U_j + t_j\right) \tag{12}$$

For every neuron, *j*, in a layer, each of the *i* inputs, $X_i$, to that layer is multiplied by a previously established weight, $w_{ij}$. These are all summed together, resulting in the internal value of this operation, $U_j$. This value is then biased by a previously established threshold value, $t_j$, and sent through an activation function, $F_{th}$. This activation function can take several forms such as Step, Linear, Sigmoid, Hyperbolic, and Gaussian functions. The Hyperbolic function, used in this study, is shaped exactly as the Sigmoid one with the same mathematical representation, as in equation 3, but it ranges from – 1 to + 1 rather than from 0 to 1 as in the Sigmoid one (Fig. 6)

$$f(x) = \frac{1}{1+e^{-x}} \tag{13}$$

The resulting output, $Y_j$, is an input to the next layer or it is a response of the neural network if it is the last layer. In applying the Neural Network technique, in this study, Neuralyst Software, Shin [20], was used.

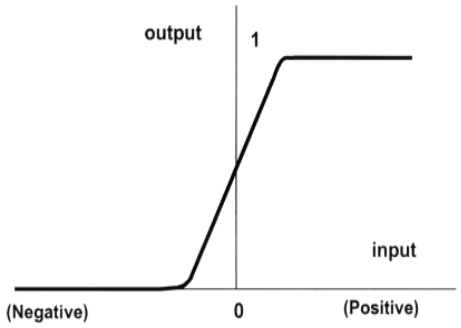


**FIGURE 6:** The Sigmoid Activation Function

### 5.2 Neural Network Training

The next step in neural network procedure is the training operation. The main purpose of this operation is to tune up the network to what it should produce as a response. From the difference between the desired response and the actual response, the error is determined and a portion of it is back propagated through the network. At each neuron in the network, the error is used to adjust the weights and the threshold value of this neuron. Consequently, the error in the network will be less for the same inputs at the next iteration. This corrective procedure is applied continuously and repetitively for each set of inputs and corresponding set of outputs. This procedure will decrease the individual or total error in the responses to reach a desired tolerance.

Once the network reduces the total error to the satisfactory limit, the training process may stop. The error propagation in the network starts at the output layer with the following equations:

$$w_{ij} = w_{ij}^{'} + LR\left(e_j X_i\right) \tag{14}$$

And,

$$e_j = Y_j\left(1 - Y_j\right)\left(d_j - Y_j\right) \tag{15}$$

Where, $w_{ij}$ is the corrected weight, $w'_{ij}$ is the previous weight value, LR is the learning rate, $e_j$ is the error term, $X_i$ is the $i^{th}$ input value, $Y_j$ is the output, and $d_j$ is the desired output.

## 6. NUMERICAL SIMULATION CASES

To fully investigate numerically the biodynamic response behaviors of seated human body subject to whole body vibration, several simulation cases are considered in this study. These simulation cases can be divided into two groups to simulate the response behaviors due to changing of human body's mass and stiffness respectively. From the analytic investigation, it is clear that the effect of damping coefficient is opposite to the effect of stiffness coefficient on the response behaviors of the human body. So in the numerical analysis, the effect of stiffness coefficient will be studied only in addition with the effect of human body's mass.

### 6.1 Neural Network Design

To develop a neural network model to simulate the effect of mass and stiffness on the biodynamic response behaviors of seated human body, first input and output variables have to be determined. Input variables are chosen according to the nature of the problem and the type of data that would be collected. To clearly specify the key input variables for each neural network simulation group and their associated outputs, Tables 2 and 3 are designed to summarize all neural network key input and output variables for the first and second simulation groups respectively.

It can be noticed from Tables 2 and 3 that every simulation group consists of three simulation cases (three neural network models) to study the effect of mass and stiffness on the seat-to-head transmissibility (STHT), driving point mechanical impedance (DPMI) and apparent mass (APMS).

| Simulation Case | Input Variables | | | | | Output |
|---|---|---|---|---|---|---|
| **STHT** | $m_1$ | $m_2$ | $m_3$ | $m_4$ | Frequency | STHT |
| **DPMI** | | | | | | DPMI |
| **APMS** | | | | | | APMS |

**TABLE 2:** Key input and output variables for the first neural network simulation group (effect of human body's mass)

| Simulation Case | Input Variables | | Output |
|---|---|---|---|
| **STHT** | $k_4$ | Frequency | STHT |
| **DPMI** | | | DPMI |
| **APMS** | | | APMS |

**TABLE 3:** Key input and output variables for the second neural network simulation group (effect of stiffness coefficient)

Several neural network architectures are designed and tested for all simulation cases investigated in this study to finally determine the best network models to simulate, very accurately, the effect of mass and stiffness based on minimizing the Root Mean Square Error (RMS-Error). Fig. 7 shows a schematic diagram for a generic neural network. The training procedure for the developed ANN models, in the current study, uses the data from the results of the analytical model to let the ANN understands the behaviors. After sitting finally the ANN models, these models are used to predict the biodynamic response behaviors for different masses and stiffness rather than those used in the analytic solution.

Table 4 shows the final neural network models for the two simulation groups and their associate number of neurons. The input and output layers represent the key input and output variables described previously for each simulation group.

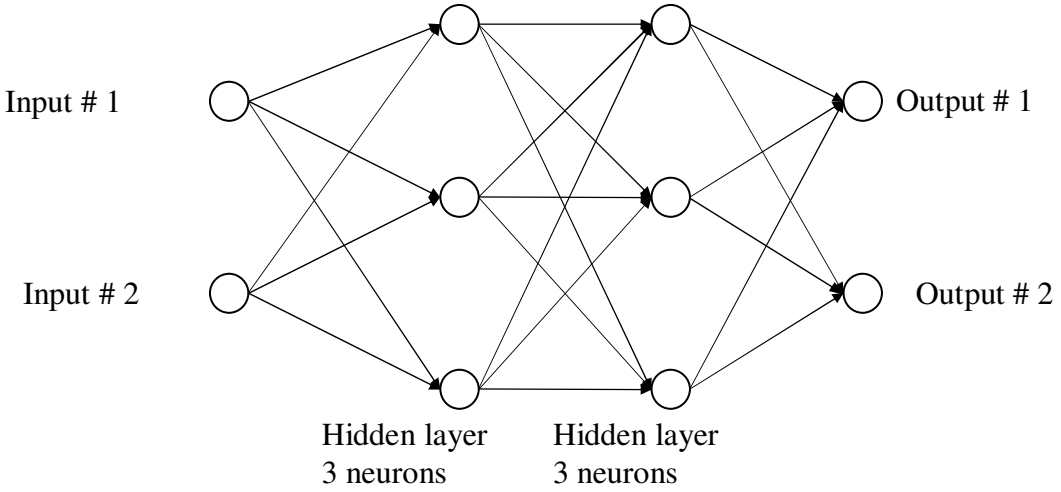


**FIGURE 7:** General schematic diagram of a simple generic neural network

| Simulation Group | | No. of Layers | No. of Neurons in each Layer | | | | |
|---|---|---|---|---|---|---|---|
| | | | Input Layer | First Hidden | Second Hidden | Third Hidden | Output Layer |
| First Group (mass) | STHT | 5 | 5 | 6 | 4 | 2 | 1 |
| | DPMI | 4 | 5 | 6 | 4 | - | 1 |
| | APMS | | | | | | |
| Second Group (Stiffness) | STHT | 4 | 2 | 5 | 3 | - | 1 |
| | DPMI | | | | | | |
| | APMS | | | | | | |

**TABLE 4:** The developed neural network models for all the simulation cases

The parameters of the various network models developed in the current study for the different simulation models are presented in table 5. These parameters can be described with their tasks as follows:

**Learning Rate (LR)**: determines the magnitude of the correction term applied to adjust each neuron's weights during training process = 1 in the current study.
**Momentum (M)**: determines the "life time" of a correction term as the training process takes place = 0.9 in the current study.
**Training Tolerance (TRT)**: defines the percentage error allowed in comparing the neural network output to the target value to be scored as "Right" during the training process = 0.001 in the current study.
**Testing Tolerance (TST)**: it is similar to Training Tolerance, but it is applied to the neural network outputs and the target values only for the test data = 0.003 in the current study.
**Input Noise (IN)**: provides a slight random variation to each input value for every training epoch = 0 in the current study.

**Function Gain (FG)**: allows a change in the scaling or width of the selected function = 1 in the current study.
**Scaling Margin (SM)**: adds additional headroom, as a percentage of range, to the rescaling computations used by Neuralyst Software, Shin (1994), in preparing data for the neural network or interpreting data from the neural network = 0.1 in the current study.
**Training Epochs**: number of trails to achieve the present accuracy.
**Percentage Relative Error (PRR)**: percentage relative error between the numerical results and actual measured value and is computed according to equation (16) as follows:

$$PRE = (\text{Absolute Value } (ANN\_PR - AMV)/AMV)*100 \quad (16)$$

Where :
ANN_PR : Predicted results using the developed ANN model
AMV : Actual Measured Value
MPRE: Maximum percentage relative error during the model results for the training step.

| Simulation Group | | Training Epochs | MPRE | RMS-Error |
|---|---|---|---|---|
| First Group (mass) | STHT | 45931 | 1.213 | 0.0015 |
| | DPMI | 7560 | 2.609 | 0.0022 |
| | APMS | 7174 | 3.743 | 0.0023 |
| Second Group (Stiffness) | STHT | 14012 | 3.449 | 0.0014 |
| | DPMI | 100185 | 3.938 | 0.002 |
| | APMS | 101463 | 1.644 | 0.0012 |

**TABLE 5:** Parameters used in the developed neural network models

## 7. NUEMERICAL RESULTS AND DISCUSSIONS

Numerical results using ANN technique will be presented in this section for the two groups (six models) to show the simulation and prediction powers of ANN technique for the effect of human body's mass and stiffness coefficient on the biodynamic response behaviors (STHT, DPMI and APMS) subject to whole-body vibration.

### 7.1 Effect of human body's mass

Three ANN models are developed to simulate and predict the effect of human body's mass on the biodynamic response behaviors (STHT, DPMI and APMS). Figures 8, 9, and 10 show the ANN results and analytical ones for different human body's masses. From ANN training figures (*Left*), it is very clear that ANN understands and simulates very well the biodynamic response behaviors. After that the developed ANN models used very successfully and efficiently to predict the response behaviors for different masses rather than those used in the analytic solution as shown in the predicted figures of ANN results (*Right*).

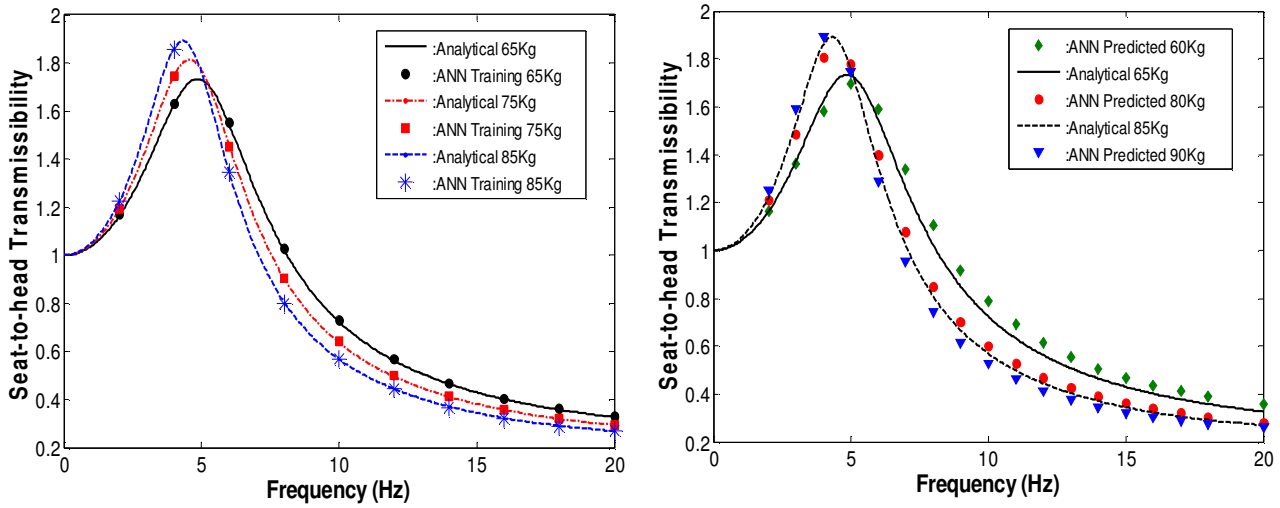


**FIGURE 8:** ANN results for the effect of human body's mass on STHT
(*Left* : ANN Training, *Right* : ANN Prediction)

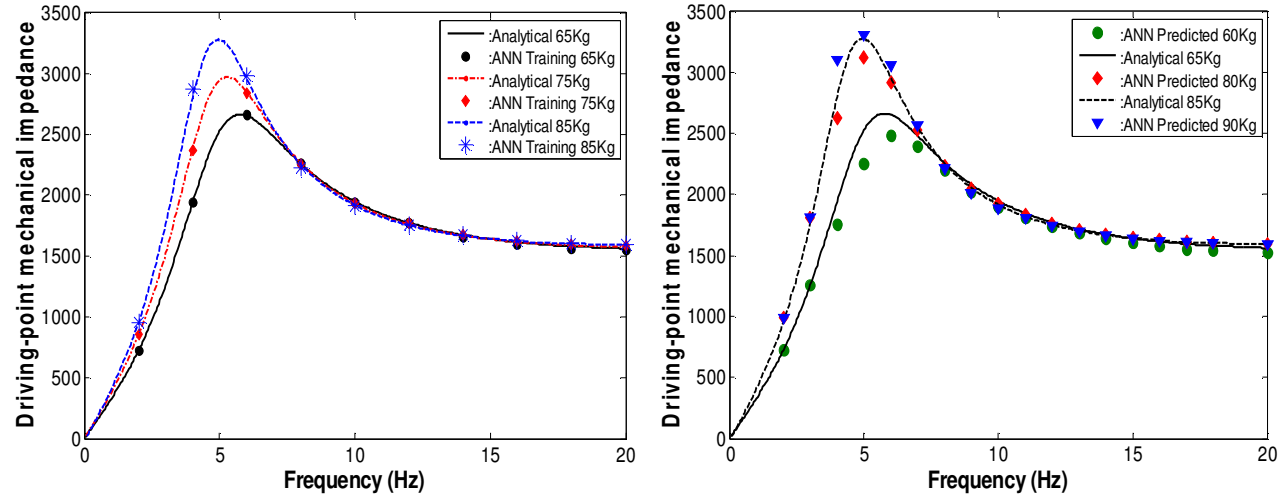


**FIGURE 9:** ANN results for the effect of human body's mass on DPMI
(*Left* : ANN Training, *Right* : ANN Prediction)

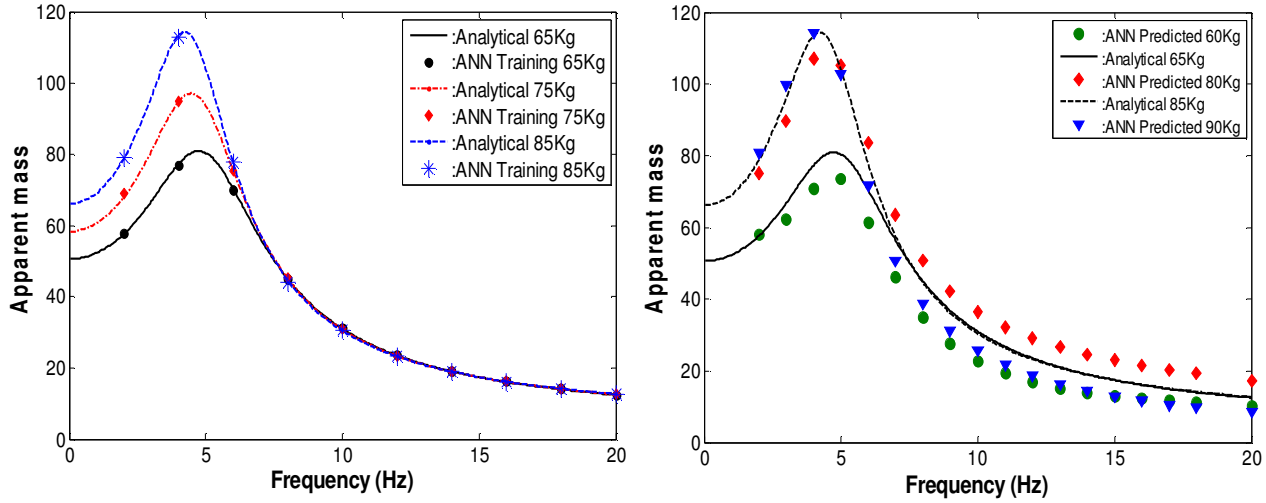


**FIGURE 10:** ANN results for the effect of human body's mass on APMS
(*Left* : ANN Training, *Right* : ANN Prediction)

### 7.2 Effect of stiffness coefficient

Another three ANN models are developed in this sub-section to simulate and predict the effect of stiffness coefficient ($k_4$) on the biodynamic response behaviors (STHT, DPMI and APMS). Figures 11, 12, and 13 show the ANN results and analytical ones for different values of $k_4$. From ANN training figures (*Left*), it is very clear that ANN understands and simulates very well the biodynamic response behaviors. After that the developed ANN models used very successfully and efficiently to predict the response behaviors for different values of $k_4$ rather than those used in the analytic solution as shown in the predicted figures of ANN results(*Right*).

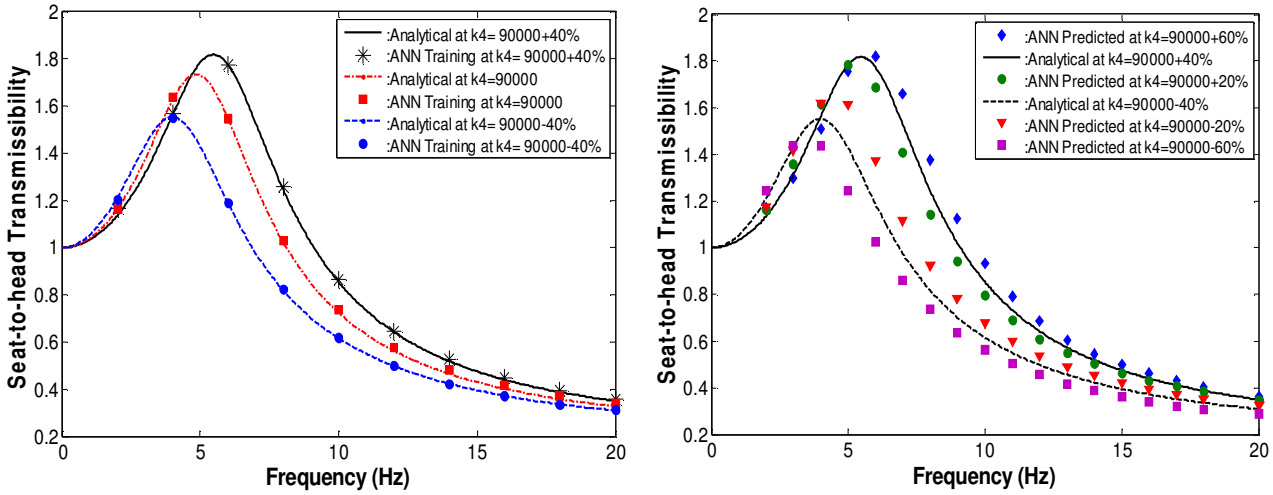


**FIGURE 11:** ANN results for the effect stiffness coefficient on STHT
(*Left* : ANN Training, *Right* : ANN Prediction)

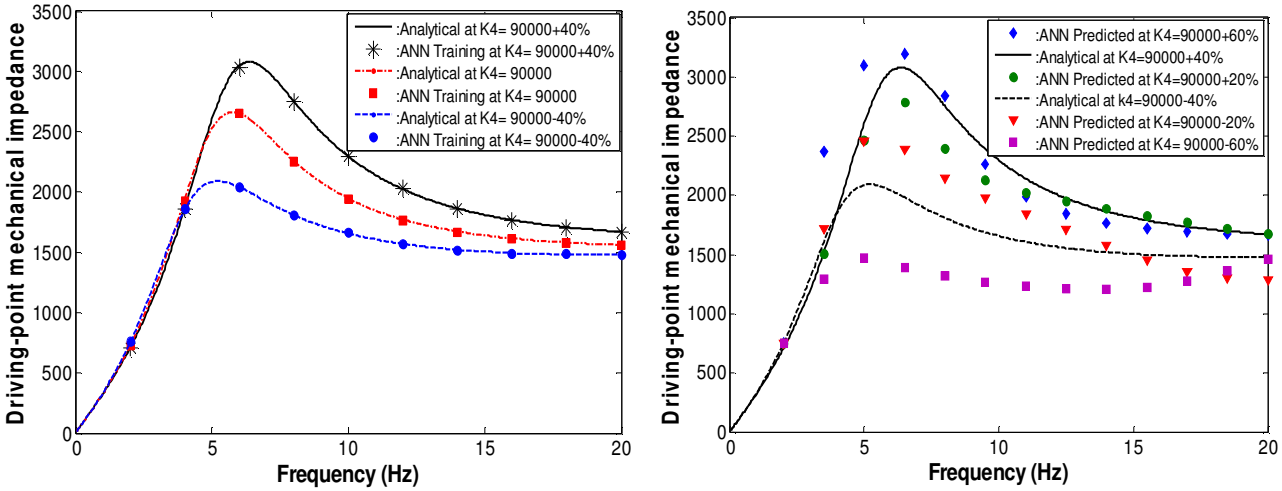


**FIGURE12:** ANN results for the effect stiffness coefficient on DPMI
(*Left* : ANN Training, *Right* : ANN Prediction)

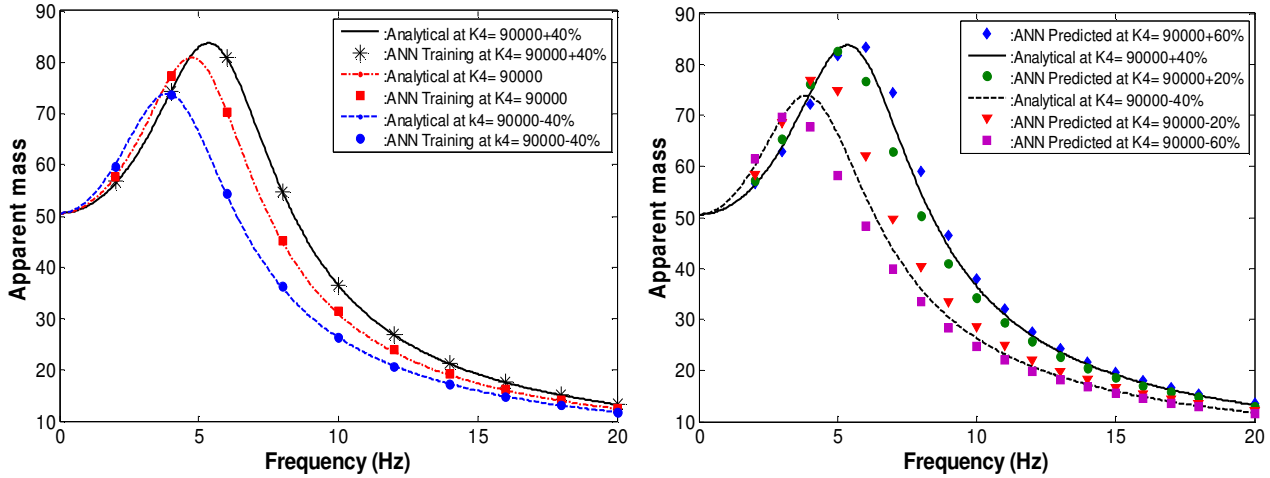


**FIGURE 13:** ANN results for the effect stiffness coefficient on APMS
(*Left* : ANN Training, *Right* : ANN Prediction)

## 8. CONCLUSIONS

Based on the analytical investigation conducted in the course of the current research, it could be concluded that the change in human body's mass, pelvic stiffness, and pelvic damping coefficient give a remarkable change in biodynamic response behaviors of seated human body (direct proportional for human body's mass and pelvic stiffness coefficient and inverse proportional for pelvic damping coefficient.)

Based on the results of implementing the ANN technique in this study, the following can be concluded:

1. The developed ANN models presented in this study are very successful in simulating the effect of human body's mass and stiffness on the biodynamic response behaviors under whole-body vibration.
2. The presented ANN models are very efficiently capable of predicting the response behaviors at different masses and stiffness rather than those used in the analytic solution.

## 9. REFERENCES

1. Wu X., Rakheja S., and Boileau P.-E., "Analyses of relationships between biodynamic response functions", Journal of Sound and Vibration, Vol. 226, No. 3, PP.595-606, 1999.

2. Coermann R. R., "The mechanical impedance of the human body in sitting and standing position at low frequencies", Human Factors, 227–253, October 1962.

3. Vogt H. L., Coermann R. R., and Fust H. D., "Mechanical impedance of the sitting human under sustained acceleration", Aerospace medicine, Vol. 39, PP. 675-679, 1968.

4. Suggs C.W., Abrams C. F., and Stikeleather L. F., "Application of a damped spring-mass human vibration simulator in vibration testing of vehicle seats", Ergonomics, Vol. 12, PP. 79–90, 1969.

5. Fairley T.E., and Griffin M.J., ''The apparent mass of the seated human body: vertical vibration'' Journal of Biomechanics Vol. 22, No 2, PP. 81–94, 1989.

6. Boileau, P.E., Rakheja, S., Yang X., and Stiharu I.,"Comparison of biodynamic response characteristics of various human body models as applied to seated vehicle drivers", Noise and Vibration Worldwide Vol. 28 ,PP. 7–14, 1997.

7. Toward M.G.R., ‘’Apparent mass of the seated human body in the vertical direction: effect of holding a steering wheel’’, In Proceedings of the 39th United Kingdom Group, Meeting on Human Response to Vibration, Ludlow, 15–17, pp 211–221, 2004.

8. Wang W., Rakhejaa S., and Boileau P.E., "Relationship between measured apparent mass and seat-to-head transmissibility responses of seated occupants exposed to vertical vibration", Journal of Sound and Vibration, Vol. 314, PP. 907-922, 2008.

9. Steina G. J., Mucka P., Hinz B., and Bluthner R., "Measurement and modeling of the y-direction apparent mass of sitting human body–cushioned seat system" Journal of Sound and Vibration, Vol. 322, PP. 454-474, 2009.

10. Tewari V. K., and Prasad N., "Three-DOF modelling of tractor seat-operator system", Journal of Terramechanics, Vol. 36, pp. 207-219, 1999.

11. Boileau, P.E., and Rakheja, S., "Whole-body vertical biodynamic response characteristics of the seated vehicle driver: Measurement and model development", International Journal of Industrial Ergonomics, Vol. 22, pp. 449-472, 1998.

12. Ramanitharan, K. and C. Li, “Forecasting Ocean Waves Using Neural Networks”, Proceeding of the Second International Conference on Hydroinformatics, Zurich, Switzerland, 1996

13. Abdeen, M. A. M., “Neural Network Model for predicting Flow Characteristics in Irregular Open Channel”, Scientific Journal, Faculty of Engineering-Alexandria University, 40 (4), pp. 539-546, Alexandria, Egypt, 2001.

14. Allam, B. S. M., “Artificial Intelligence Based Predictions of Precautionary Measures for building adjacent to Tunnel Rout during Tunneling Process” Ph.D., 2005.

15. Azmathullah, H. Md., M. C. Deo, and P. B. Deolalikar, “Neural Networks for Estimation of Scour Downstream of a Ski-Jump Bucket", Journal of Hydrologic Engineering, ASCE, Vol. 131, Issue 10, pp. 898-908, 2005.

16. Abdeen, M. A. M., “Development of Artificial Neural Network Model for Simulating the Flow Behavior in Open Channel Infested by Submerged Aquatic Weeds”, Journal of Mechanical Science and Technology, KSME Int. J., Vol. 20, No. 10, Soul, Korea, 2006

17. Mohamed, M. A. M., “Selection of Optimum Lateral Load-Resisting System Using Artificial Neural Networks”, M. Sc. Thesis, Faculty of Engineering, Cairo University, Giza, Egypt, 2006.

18. Abdeen, M. A. M., “Predicting the Impact of Vegetations in Open Channels with Different Distributaries’ Operations on Water Surface Profile using Artificial Neural Networks”, Journal of Mechanical Science and Technology, KSME Int. J., Vol. 22, pp. 1830-1842, Soul, Korea, 2008.

19. Boileau P.E., "A study of secondary suspensions and human drivers response to whole-body vehicular vibration and shock", PhD. Thesis, Concordia university, Montreal, Quebec, Canada, 1995.

20. Shin, Y., “Neuralyst$^{IM}$ User’s Guide”, “Neural Network Technology for Microsoft Excel”, Cheshire Engineering Corporation Publisher, 1994

# CALL FOR PAPERS

**Journal:** International Journal of Engineering (IJE)
**Volume:** 5 **Issue:** 1
**ISSN:**1985-1553
**URL:** http://www.cscjournals.org/csc/description.php?JCode=IJE

International Journal of Engineering (IJE) is devoted in assimilating publications that document development and research results within the broad spectrum of subfields in the engineering sciences. The journal intends to disseminate knowledge in the various disciplines of the engineering field from theoretical, practical and analytical research to physical implications and theoretical or quantitative discussion intended for both academic and industrial progress.

Our intended audiences comprises of scientists, researchers, mathematicians, practicing engineers, among others working in Engineering and welcome them to exchange and share their expertise in their particular disciplines. We also encourage articles, interdisciplinary in nature. The realm of **International Journal of Engineering (IJE)** extends, but not limited, to the following:

To build its International reputation, we are disseminating the publication information through Google Books, Google Scholar, Directory of Open Access Journals (DOAJ), Open J Gate, ScientificCommons, Docstoc and many more. Our International Editors are working on establishing ISI listing and a good impact factor for IJE.

**IJE List of Topics:**

The realm of International Journal of Engineering (IJE) extends, but not limited, to the following:

- Aerospace Engineering
- Agricultural Engineering
- Biomedical Engineering
- Chemical Engineering
- Civil & Structural Engineering
- Computer Engineering
- Control Systems Engineering
- Education Engineering
- Electrical Engineering
- Electronic Engineering
- Engineering Mathematics
- Engineering Science
- Environmental Engineering
- Fluid Engineering
- Geotechnical Engineering
- Industrial Engineering
- Manufacturing Engineering
- Materials & Technology Engineering
- Mechanical Engineering
- Mineral & Mining Engineering

- Nuclear Engineering
- Petroleum Engineering
- Telecommunications Engineering
- Optical Engineering
- Robotics & Automation Engineering

## IMPORTANT DATES

**Volume:** 5
**Issue:** 1
**Paper Submission:** January 31, 2011
**Author Notification:** March 01, 2011
**Issue Publication:** March /April 2011

# CALL FOR EDITORS/REVIEWERS

CSC Journals is in process of appointing Editorial Board Members for ***International Journal of Engineering (IJE)***. CSC Journals would like to invite interested candidates to join **IJE** network of professionals/researchers for the positions of Editor-in-Chief, Associate Editor-in-Chief, Editorial Board Members and Reviewers.

The invitation encourages interested professionals to contribute into CSC research network by joining as a part of editorial board members and reviewers for scientific peer-reviewed journals. All journals use an online, electronic submission process. The Editor is responsible for the timely and substantive output of the journal, including the solicitation of manuscripts, supervision of the peer review process and the final selection of articles for publication. Responsibilities also include implementing the journal's editorial policies, maintaining high professional standards for published content, ensuring the integrity of the journal, guiding manuscripts through the review process, overseeing revisions, and planning special issues along with the editorial team.

A complete list of journals can be found at http://www.cscjournals.org/csc/byjournal.php. Interested candidates may apply for the following positions through http://www.cscjournals.org/csc/login.php.

*Please remember that it is through the effort of volunteers such as yourself that CSC Journals continues to grow and flourish. Your help with reviewing the issues written by prospective authors would be very much appreciated.*

Feel free to contact us at coordinator@cscjournals.org if you have any queries.

# Contact Information

**Computer Science Journals Sdn BhD**
M-3-19, Plaza Damas Sri Hartamas
50480, Kuala Lumpur MALAYSIA

Phone: +603 6207 1607
+603 2782 6991
Fax: +603 6207 1697

**BRANCH OFFICE 1**
Suite 5.04 Level 5, 365 Little Collins Street,
MELBOURNE 3000, Victoria, AUSTRALIA

Fax: +613 8677 1132

**BRANCH OFFICE 2**
Office no. 8, Saad Arcad, DHA Main Bulevard
Lahore, PAKISTAN

**EMAIL SUPPORT**
Head CSC Press: coordinator@cscjournals.org
CSC Press: cscpress@cscjournals.org
Info: info@cscjournals.org

COMPUTER SCIENCE JOURNALS SDN BHD
M-3-19, PLAZA DAMAS
SRI HARTAMAS
50480, KUALA LUMPUR
MALAYSIA